2012

Materials selection, processing, and manufacturing for a design of an elbow joint replacement prototype

Erik Manatt
Iowa State University

Materials selection, processing, and manufacturing for a design of an elbow joint replacement prototype

by

Erik Michael Manatt

A thesis submitted to the graduate faculty
in partial fulfillment of the requirements for the degree of
MASTER OF SCIENCE

Major: Materials Science and Engineering

Program of Study Committee:
Richard A. LeSar, Major Professor
Thomas D. McGee
William D. Hoefle

Iowa State University
Ames, Iowa
2012

TABLE OF CONTENTS

LIST OF TABLES

LIST OF FIGURES

ABSTRACT

A new design for a canine elbow joint replacement was manufactured and assembled. The design incorporates a ceramic ball for articulation with radius and ulna components and a bioactive ceramic for tissue contact. A variety of materials were considered, with zirconia-toughened alumina selected as the wear surface, stainless steel as the structural backbone, and osteoceramic as the bioactive bone interface. The ceramic components were manufactured by cold isostatic pressing the powders, firing the formed rods to an intermediate temperature for strength, and then machining them before a final sintering. A modified osteoceramic bone cement with better flow characteristics was chosen instead of poly(methylmethacrylate) bone cement for fixation of the ulna component.

INTRODUCTION

Elbow replacement surgeries are much less common than hip replacements and therefore have received less attention from researchers. Two possible reasons for replacing an elbow joint are rheumatoid arthritis or posttraumatic arthritis, usually with significant bone loss [1]. The most common practice for elbow replacement is to cement separate rods into the humerus and ulna and attach them through a hinge joint.

Current elbow implants have improved the quality of life for many human patients; however, the five year survival rate for a common implant of this type (Coonrad-Morrey total elbow replacement) is only 72% [1]. Poly(methylmethacrylate) (PMMA), the bone cement used to hold the implant in the medullary cavity of the humerus and ulna, has significant problems of as well, including tissue necrosis due to high setting temperature and monomer toxicity [2]. Loose particles of PMMA in living tissue also invoke a negative foreign-body response.

Elbow implants can be constrained (simple hinge), semi-constrained (loose hinge), or unconstrained (articulating components held together by soft tissue) [3]. Constrained implants are no longer commonly used because of high failure rates due to aseptic loosening [1]. Loosening in constrained implants is caused by the rotational forces borne by the hinge and thus the bone cement [3]. Unconstrained implants, and to a lesser extent semi-constrained implants, are less likely to experience aseptic loosening because the surrounding living tissue supports these forces; however, maintaining stability is a concern with unconstrained implants [1,3]. Semi-constrained implants are “used in many centers and are used routinely by some surgeons” while unconstrained implants have seen little use due to the aforementioned concerns [1].

There is a need for an elbow implant that effectively transfers load to bone, maintains as much living bone as possible, and minimizes negative foreign body response. This implant should be unconstrained, utilize a material to which bone bonds for support, and articulate on a wear resistant ceramic to prevent the release of hazardous wear particles. Such an implant has been designed by Dr. Thomas McGee.

Research Objective

The goals of this research are to select the necessary materials and processing techniques, and to manufacture and assemble a ball-centered elbow joint replacement prototype. Bone physiology must be considered to ensure a safe and effective implantation.

Ultimately, this implant will be adapted for use in humans; however, to ensure its safety and effectiveness it should be first tested in animals. Canines are the most logical choice for this research because the surgeons at the Iowa State College of Veterinary Medicine are familiar with canines and the structure of the canine elbow joint (as shown in [4]) is similar to the elbow joint in humans (as shown in [5]). The development of this new ball-centered elbow joint prototype has not yet advanced to the point to begin live trials, but cadaver elbow joints have been examined for inspiration.

LITERATURE REVIEW

Use of Animals in Orthopaedic Research [6]

The use of animal models in orthopaedic research is important to ensure safe performance in human clinical trials after in vitro studies have proven successful. Animal models should only be used in circumstances where the information cannot be gained in any other way and provides insight into future human trials. Care must be taken to prevent extraordinary pain or disability to the animal. The knowledge gleaned from animal models can provide immense benefit to both humans and animals.

An and Friedman give six considerations when selecting an animal for orthopaedic research: ethics, availability, housing requirements, ease of handling, cost, and susceptibility to disease. With ethics in mind, it is important to use the most primitive animal that will provide the desired information. Pain, disability, and/or distress to the animal must be minimized. Generally, in the United States, availability of animals is not a concern. Housing for a research animal must be provided so the types of animals that can be used for an experiment will depend on the available facilities. The animals could be housed elsewhere, however there is great benefit to being able to easily visit and inspect the animals. Ease of handling is one of the main reasons that small animals are used more commonly in research than large animals. In certain cases, larger bones, muscles, or tendons are necessary, which requires the use of a larger animal. Cost, including transportation, housing, etc., should not be a decisive factor in choosing an animal, however a cheaper animal can be used, provided sufficient data can be obtained. Many animals are prone to certain diseases and this should be taken into account before embarking on a long-term study. An ill animal can distort data and increase total cost. In some cases it is possible to purchase disease-resistant animals.

For the research performed in this thesis, a cadaver canine was used. The materials used in the implant have already been proven to be biocompatible, so testing in a living organism at this stage is unnecessary. Cadaver canines are relatively easy to obtain from the Iowa State Veterinary Hospital and provide bones large enough to give a reasonable comparison to human bone.

Anatomy of Bone

Composition of Bone

Bone owes its unique combination of strength, durability, and flexibility to a composite matrix of organic and inorganic components. As shown in Table 1, just over two-thirds of bone is made up of apatite crystals, which gives bone its hardness [5]. The crystals tend to be shaped like spindles (20-40nm by 1.5-3nm) or plates and reside around and throughout the collagen fibers [7]. The mineral component is very nearly hydroxyapatite ($Ca_{10}(PO_4)_6(OH)_2$); however, the apatite has a number of impurities including citrate ($C_6H_5O_7^{-4}$), carbonate (CO_3^{-2}), fluoride (F), and hydroxyl ions (OH^-) [7]. The organic component is primarily composed of osteoid, which includes proteoglycans, glycoproteins, and collagen fibers [5]. As discussed later in the structure of osteons, collagen fibers are responsible for the bone's tensile and torsional strength.

Table 1: Composititon of bone. [7] from original source [8]

Component	***Amount (wt.%)***
Mineral (Apatite)	69
Organic Matrix	22
Collagen	(90-96% of organic matrix)
Others	(4-10% of organic matrix)
Water	9

Structure of Bone [5]

Bones have high strength and low weight due to their structure based on two "types" of bone: compact and cancellous (or spongy). Compact bone is dense, while cancellous bone, with its sponge- or honeycomb-like structure, is much less dense and contains marrow. A typical long bone, such as the femur, has compact bone all around the surface with cancellous bone filling in the space at the ends of the bone, known as the epiphyses. In the diaphysis, or shaft, of a long bone is the medullary cavity which holds the marrow.

The surface of compact bone is covered by a white, double layered membrane called the periosteum. The periosteum is fixed to the bone matrix by a web of collagen fibers called Sharpey's fibers. Numerous nerves, fibers, and blood vessels supply the periosteum, which

has openings throughout to provide innervation and nutrition to the bone. Cancellous bone, along with internal bone surfaces, is covered by a similar membrane known as the endosteum. Both membranes contain cells known as osteoblasts and osteoclasts (discussed in Physiology of Bone section). Surfaces where the bone contacts other bone(s) are usually covered by cartilage, shown as light blue in Figure 1. Cartilage is similar to bone, but receives no blood supply and therefore heals poorly [9].

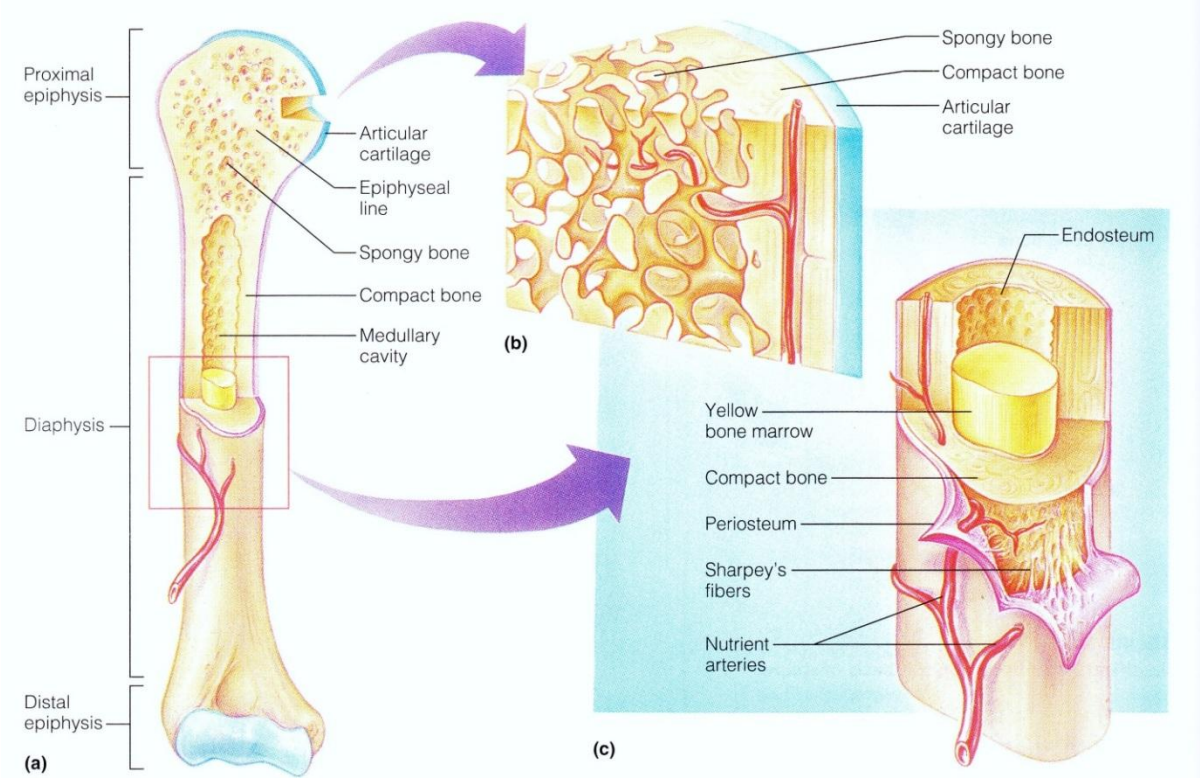

Figure 1: Compact and spongy bone in a long bone. [5]

Compact bone can be broken down into structural units known as osteons or Haversian systems. At the center of each osteon there is a canal that innervates and supports the flow of nutrients via blood to the bone. The osteons are cylindrically shaped (200-250μm diameter) with their long axis parallel to the long axis of the bone and are formed by separate layers of collagen known as lamellae (3-7μm wide) [10]. The collagen fibers in each lamella run in the same direction but the collagen fibers in neighboring lamellae run in the opposite direction which helps the bone withstand torsional stresses. In between the lamellae are

osteocytes which lie in small pockets called lacunae. The osteocytes help to maintain the bone matrix. Canaliculi, which are small channels, run through the lamellae from the central canal to all of the lacunae.

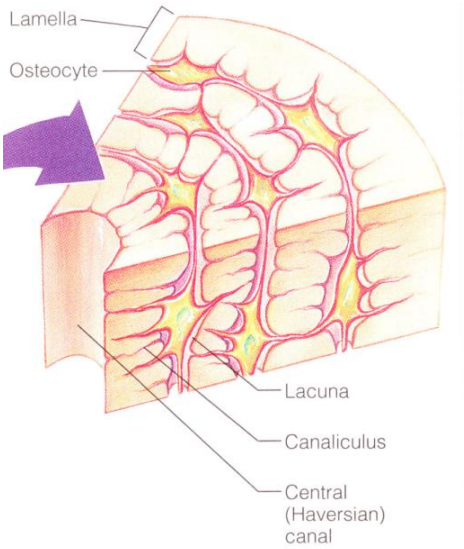

Figure 2: A pie shaped slice of an osteon. Adapted from [5]

Trabeculae, which make up the sponge-like structure of cancellous bone, are not oriented randomly, but rather are aligned to best support the stresses imposed upon the bone. The trabeculae are also composed of lamellae with canaliculi and osteocytes. Cancellous bone does not contain osteons; however, cancellous bone does receive nutrition in a very similar manner, simply without a central canal. The nutrition comes from the marrow surrounding the trabeculae.

Mechanical Properties of Bone

A comparison of the mechanical properties of certain human and canine bones is shown below in Table 2. It is important to note that there are large discrepancies in the values reported for the mechanical properties of bone. There are a number of reasons for this disparity, including the lack of uniformity in bone and the manner in which the bone samples are stored [11]. One common procedure is to keep the bone samples wet with saline after harvesting because dried bones exhibit different properties, for example higher compressive strength [11,12].

Table 2: Comparison of human and canine bone mechanical properties in MPa. [12]

Property	*Bone*	*Human*	*Canine*	*Note*
Ultimate Compressive Strength	Femur	154	114	middle portion of the shaft in the longitudinal direction
	Humerus	125	112±2.9	
	Radius	115	—	
	Ulna	118	—	
Ultimate Bending Strength	Femur	208±7.8	165±5.9	anteroposterior direction
	Humerus	211±4.9	166±7.8	
	Radius	227±5.9	174±7.8	
	Ulna	225±4.9	174±6.9	
Ultimate Torsional Strength	Femur	45.3	65.7±3.0	human specimens were adults
	Humerus	42.6	66.6±4.3	
	Radius	48.5	74.5±6.5	
	Ulna	44.6	60.8±5.1	
Elastic Modulus	Femur	18300	11500	anteroposterior bending
	Humerus	10000	8430	
	Radius	15900	9900	
	Ulna	15400	17800	

The tests were performed with wet long bone and human specimens were 20-39 years old except where otherwise noted. All values are in units of MPa (converted from kg/mm^2).

Physiology of Bone

Remodeling of Bone [10]

Adult bone constantly undergoes a process known as remodeling. Remodeling can be thought of as bone turnover, because this process not only repairs microcracks that form in the bone, but also continuously removes and deposits bone where necessary. There are two predominant factors that control whether bone is removed or deposited. The first is Ca^{2+} homeostasis, which is essentially maintaining the proper balance of Ca^{2+} ions. The second is mechanical stress, which effects remodeling by an unknown mechanism. As shown in Figure 3, bone will deposit or resorb bone to best deal with the stresses imposed upon it, following the orthopaedic mantra attributed to Wolff's law: form follows function.

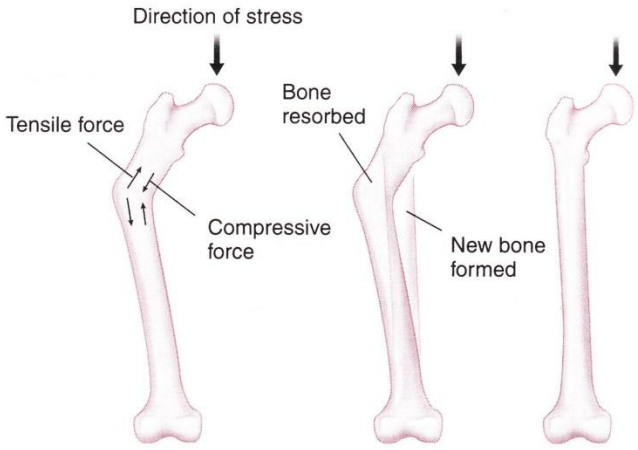

Figure 3: Wolff's law applied to a femur. Adapted from [10]

Osteoblasts are responsible for depositing new bone. Osteoid is secreted onto the bone surface and is mineralized over the next 5 to 15 days. It is currently not understood how the osteoblasts regulate the precipitation of hydroxyapatite. The resorption of bone is performed by much larger, multinucleated cells called osteoclasts, which secrete lysosomal enzymes and metabolic acids [5]. A small pit, also known as Howship's lacuna, is formed after resorption. The release of growth factors during resorption causes osteoblasts to move in and rebuild the bone after the osteoclasts move to resorb bone elsewhere. About 15% of the osteoblasts will become osteocytes in the newly formed bone matrix.

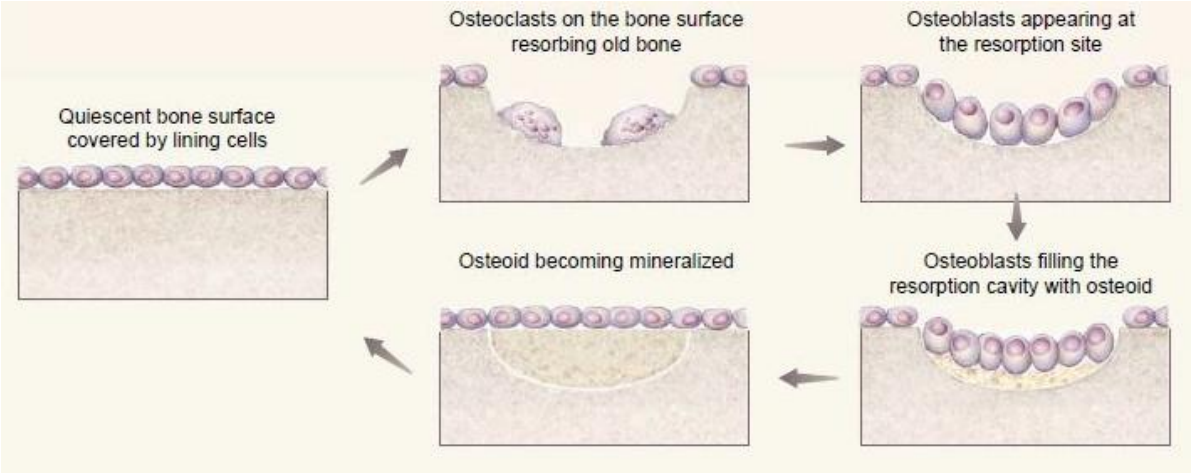

Figure 4: Remodeling of bone. Adapted from [13]

Fracture Repair [5]

According to Marieb, there are four major phases that describe the repair process for a simple fracture (clean break under the skin). The first phase is hematoma formation, due to the breaking of blood vessels in and around the bone. This phase is accompanied by swelling, pain, and inflammation.

In the second phase a fibrocartilaginous callus forms to bridge the gap in the broken bone. The fibrocartilaginous callus is a term used to describe all of the repair tissue in the gap between the bones. In this phase phagocytic cells clean up the area while capillaries grow in to supply nutrition. New bone is laid down by fibroblasts and osteoblasts. Collagen fibers to reconnect the bone ends are created by the fibroblasts while the osteoblasts start building a matrix of spongy bone. Osteoblasts further from the nutrition supply and chondroblasts, which are differentiated fibroblasts, fill the entire area with a cartilaginous matrix for increased support of the break.

The fibrocartilaginous callus dissolves and is replaced by a bony callus of cancellous bone in the third phase. This conversion is caused by the increasing numbers of osteoclasts and osteoblasts in the fibrocartilaginous callus. The bony callus usually starts to form 3-4 weeks after the injury and provides a strong connection after 2-3 months.

The fourth and final phase is characterized by remodeling of the repaired tissue. This process begins during the third phase and generally continues for several months. The inside and outside of the bone is cleaned up and compact bone is formed.

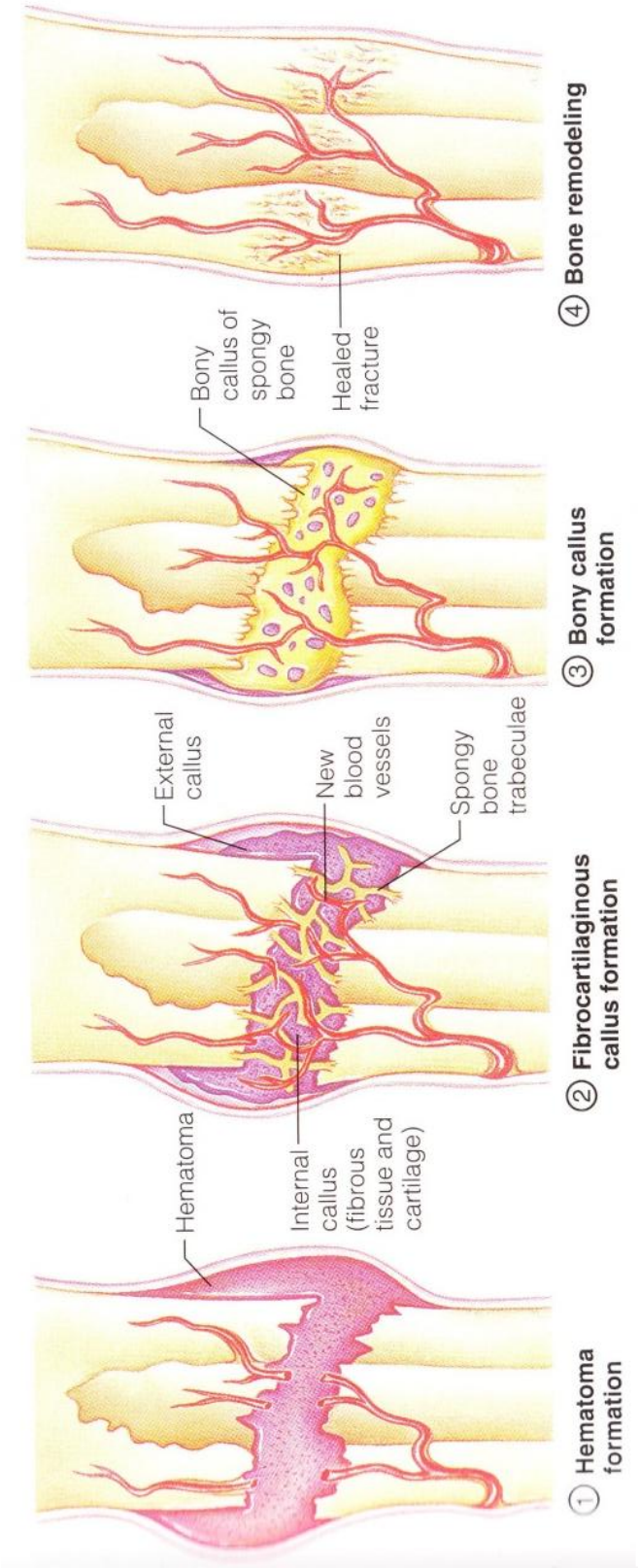

Figure 5: The phases of bone repair. [5]

The Synovial Joint [9]

There are three types of joints: fibrous (synarthroses), cartilaginous (amphiarthroses), and synovial (diarthroses). The first two allow no or very little movement while the latter allows a significant range of motion. The elbow joint is composed of three synovial sub-joints (humero-ulnar, humero-radial, and radio-ulnar) all encased in one joint capsule. The joint capsule has two layers, each with its own function. The outer layer is protective and provides strength, while the inner layer dispenses synovial fluid, a thick lubricant for the joint. Synovial fluid is also the only medium through which nutrition reaches, and waste is removed from, the cartilage in the joint. Inside the joint capsule are the joint cavity and the articulating bones. The friction between the articulating bones is reduced by hyaline cartilage, which covers the articulating surfaces.

Structure of the Elbow Joint [9]

The canine elbow is constructed of the same bones as the human elbow, albeit in slightly different orientations. The greatest difference is the location of the radius, which is on top of the ulna and inhibits the ability of canines to rotate their elbows significantly. Canine musculature and innervation around the elbow joint can be seen in Figure 7 and Figure 8.

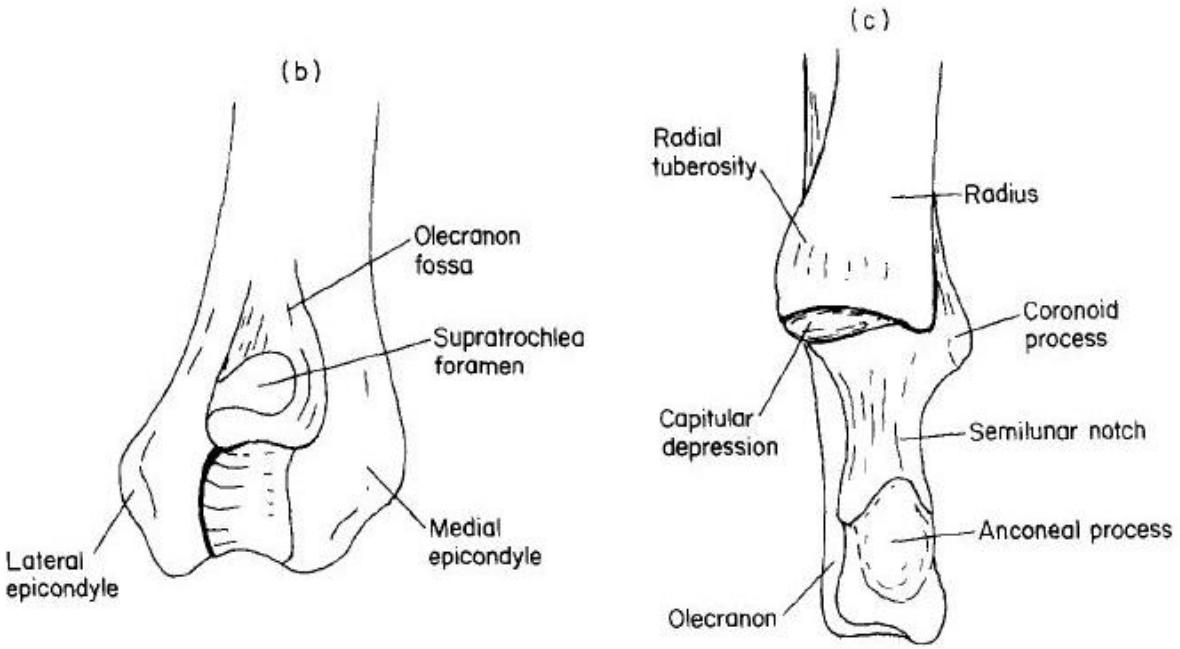

Figure 6: (b) Caudal aspect of left humerus. (c) Cranial aspect of left radius and ulna. [4]

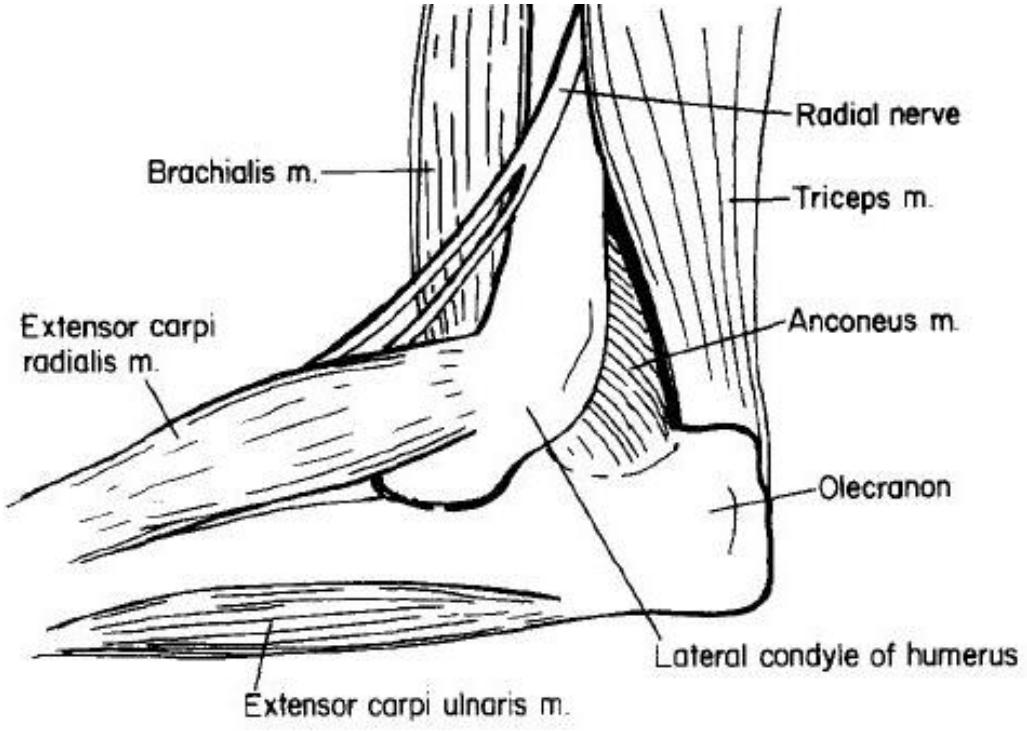

Figure 7: Lateral aspect of left elbow—soft tissue structures of surgical importance [4].

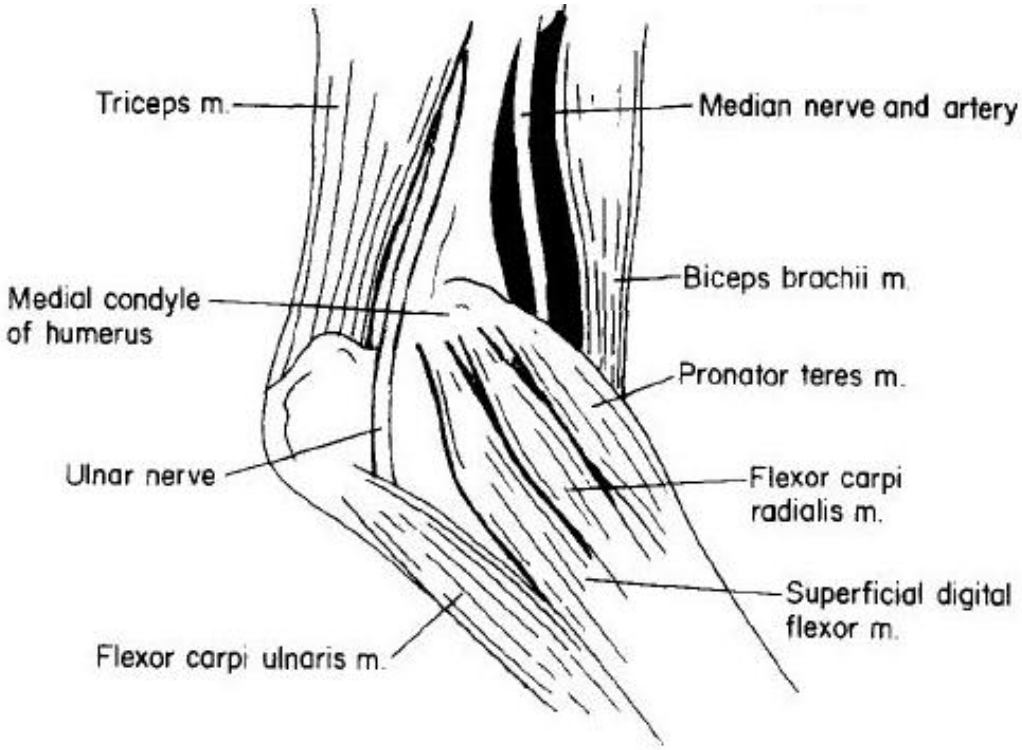

Figure 8: Medial aspect of left elbow—soft tissue structures of surgical importance [4].

The three sub-joints of the elbow each provide an important function. The humero-radial joint, between the humerus and radius, carries the majority of load experienced by the elbow. Elbow stability and the hinge-like motion of the elbow joint are maintained by the humero-ulnar joint, between the humerus and ulna [9,4]. The final elbow joint, the proximal radio-ulnar joint, is located between the radius and ulna and allows for rotation of the elbow.

The stability of joints is improved by the presence of ligaments, which are bands of connective tissue originating and terminating in bone. Ligaments, like cartilage, are avascular. This means a partially detached or torn ligament cannot heal well-enough to provide as much stability as an uninjured ligament. Lateral movement of the elbow is restrained by the collateral ligaments and the fit of the anconeal process into the olecranon fossa (see Figure 9) [4]. The annular ligament surrounds and keeps the radius against the ulna during rotation. Hyperextension of the elbow is likely resisted by the oblique ligament while separation of the olecranon and humerus is prevented by the olecranon ligament.

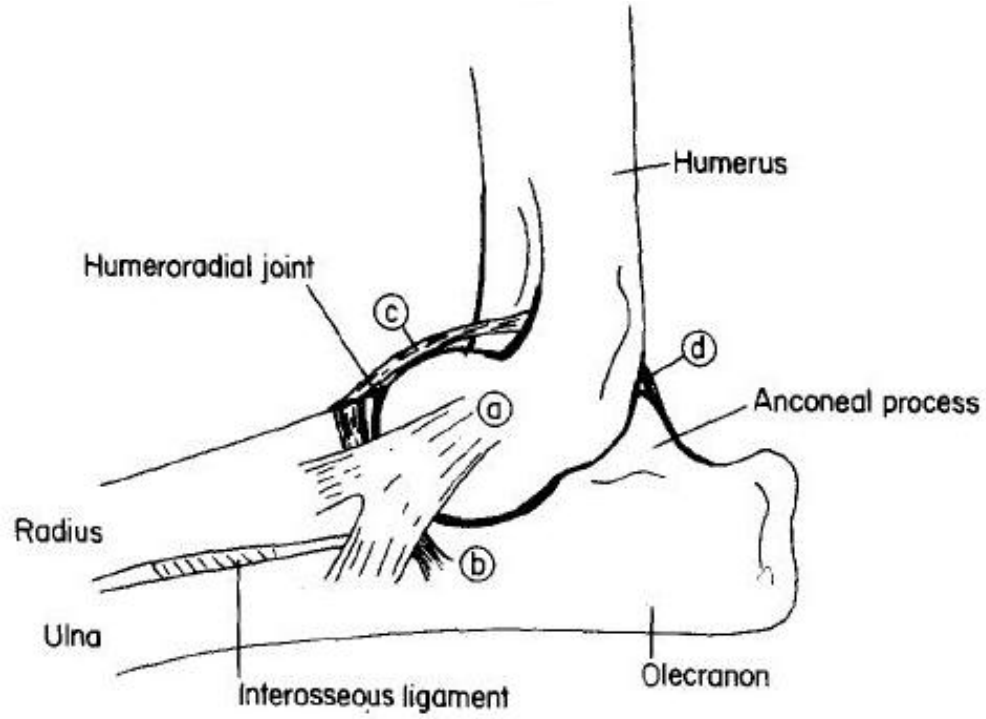

Figure 9: Lateral aspect of the left elbow: (a) Lateral collateral ligament; (b) Annular ligament; (c) Oblique ligament; (d) Olecranon ligament. [4]

Materials

For a material to be considered a biomaterial it must be able to safely and reliably replace and/or function in living tissue with an appropriate physiological response [7]. In other words, the material must be biocompatible. There are four groups of synthetic biomaterials: polymers, metals, ceramics, and composites [7]. For this research only polymers were not used, which are commonly used as the articulating surfaces and as bone cement in conventional implants. Both of these applications of polymers have been replaced with ceramics.

Alumina

Single crystal alumina is hard and strong but is too brittle to be used as an articulating component (see APPENDIX I). Like most ceramics, the strength of polycrystalline alumina can be improved by decreasing porosity and grain size [7]. Grain growth can be hindered by adding MgO (less than 0.5wt%) [14]. An alumina implant must have a flexural strength

greater than 400MPa and an elastic modulus of 380GPa to meet ASTM standards F603-78 [7]. Alumina's advantages over metals and other ceramics are its low friction surface and wear resistance, making it a useful material for articulating surfaces. Grains must be smaller than four microns with little variation in size to prevent pull-outs and maintain high wear resistance [14]. For joint implants the articulating components are polished against each other to ensure a smooth surface and a good fit. Alumina has excellent corrosion resistance and only prompts thin capsule formation.

Zirconia

Zirconia is commonly doped with magnesia and/or yttria to stabilize its higher temperature phases (tetragonal then cubic) [7]. This is necessary to prevent the large volume expansion that occurs when tetragonal or cubic zirconia transforms to the room temperature monoclinic structure [7,15]. If zirconia is not stabilized, or sintered below the tetragonal-monoclinic transformation, it will almost certainly develop cracks and fail during cooling [15].

The presence of the metastable tetragonal phase improves the fracture toughness of zirconia through crack growth retardation [7]. The stresses induced during crack propagation cause the tetragonal particles to transition to the monoclinic phase, increasing their volume and closing the crack. Yttria-stabilized zirconia (YSZ) is often used instead of alumina because of its superior fracture strength, fracture toughness, and wear resistance against ultrahigh-molecular-weight polyethylene. It is important to note, however, that an alumina-alumina articulating component wears significantly less than zirconia-zirconia. Zirconia's biocompatibility is similar to alumina.

Unfortunately, these benefits are not without side-effects: YSZ is susceptible to low-temperature degradation (LTD) in moist environments [15]. LTD causes the transformation from tetragonal to monoclinic to occur without the presence of a crack, resulting in "surface roughening, microcracking, and grain pull-out as well as loss of strength". Grain size, pore structure, and yttria content all have an effect on the likelihood of LTD occurring. Doping zirconia with certain other stabilizers, such as ceria, or using a two phase zirconia composite, such as alumina-zirconia, is an effective method to reduce susceptibility to LTD.

Table 3: Comparison of properties of alumina and zirconia. [7] from original source [16]

Property	***Alumina***	***Zirconia***
Chemical composition	Al_2O_3+MgO	ZrO_2+MgO+Y_2O_3
Purity (%)	99.9	95~97
Density (g/cm^3)	>3.97	5.74~6.0
Porosity (%)	<0.1	<0.1
Bending strength (MPa)	>500	500~1000
Compression strength (MPa)	4100	2000
Young's modulus (GPa)	380	210
Poisson's ratio	0.23	0.3
Fracture toughness (MPa*m$^{1/2}$)	4	up to 10
Thermal expansion coefficient (*10^{-6}/K)	8	11
Thermal conductivity (W/m*K)	30	2
Hardness (HV0.1)	up to 2200	1200
Contact angle (°)	10	50

Calcium Phosphates

As mentioned previously, the majority of bone is composed of minerals, most notably an impure form of hydroxyapatite. Because of this, synthesized hydroxyapatite has superb biocompatibility [7]. Stoichiometric hydroxyapatite is monoclinic [17]. It has lattice parameters a = 9.4214(8), b = 2a, c = 6.8814(7) A, $\gamma = 120°$ with a space group symmetry of $P2_1/b$. In stoichiometric hydroxyapatite, the OH^- ions form ordered columns (i.e. OH OH OH OH); however, sufficient impurities allow a disordered column structure by giving a point of reversal in the column, for example an F^- impurity would allow OH OH F HO HO. In this nonstoichiometric case the structure of hydroxyapatite is hexagonal.

Another important calcium phosphate is tricalcium phosphate. Tricalcium phosphate has a high temperature phase (α, monoclinic), and a low temperature phase (β, rhombohedral) [17]. The calcium to phosphorus (Ca:P) ratio and formula for these and other calcium phosphates can be found in Table 4. The Ca:P ratio is important because as it decreases, the solubility of the mineral in the body increases (i.e. tricalcium phosphate will dissolve faster than hydroxyapatite) [14]. The solubility isotherms of common calcium phosphates are shown in Figure 10. At the normal body pH of around 7, it is easy to see that hydroxyapatite is the most stable calcium phosphate.

The difference in solubility between hydroxyapatite and tricalcium phosphate is useful because it allows an implant or bone filler to dissolve away; however, care must be taken to ensure that the rate of dissolution is similar to the rate of new bone growth [14]. Factors that increase the rate of dissolution include: increasing surface area, decreasing crystallinity, decreasing crystal perfection, and decreasing crystal and grain size. The solubility of hydroxyapatite increases with ionic substitutions of CO_2^{-3}, Mg^{2+}, and Sr^{2+}, but decreases with F^- substitution.

Table 4: Calcium Phosphates. [14]

Ca:P	***Mineral Name***	***Formula***	***Chemical Name***
1.0	Monetite	$CaHPO_4$	Dicalcium phosphate (DCP)
1.0	Brushite	$CaHPO_4 \cdot 2H_2O$	Dicalcium phosphate dihydrate (DCPD)
1.33	-	$Ca_8(HPO_4)_2(PO_4)_4 \cdot 5H_2O$	Octocalcium phosphate (OCP)
1.43	Whitlockite	$Ca_{10}(HPO_4)(PO_4)_6$	
1.5	-	$Ca_3(PO_4)_2$	Tricalcium phosphate (TCP)
1.67	Hydroxyapatite	$Ca_{10}(PO_4)_6(OH)_2$	
2.0	-	$Ca_4P_2O_9$	Tetracalcium phosphate

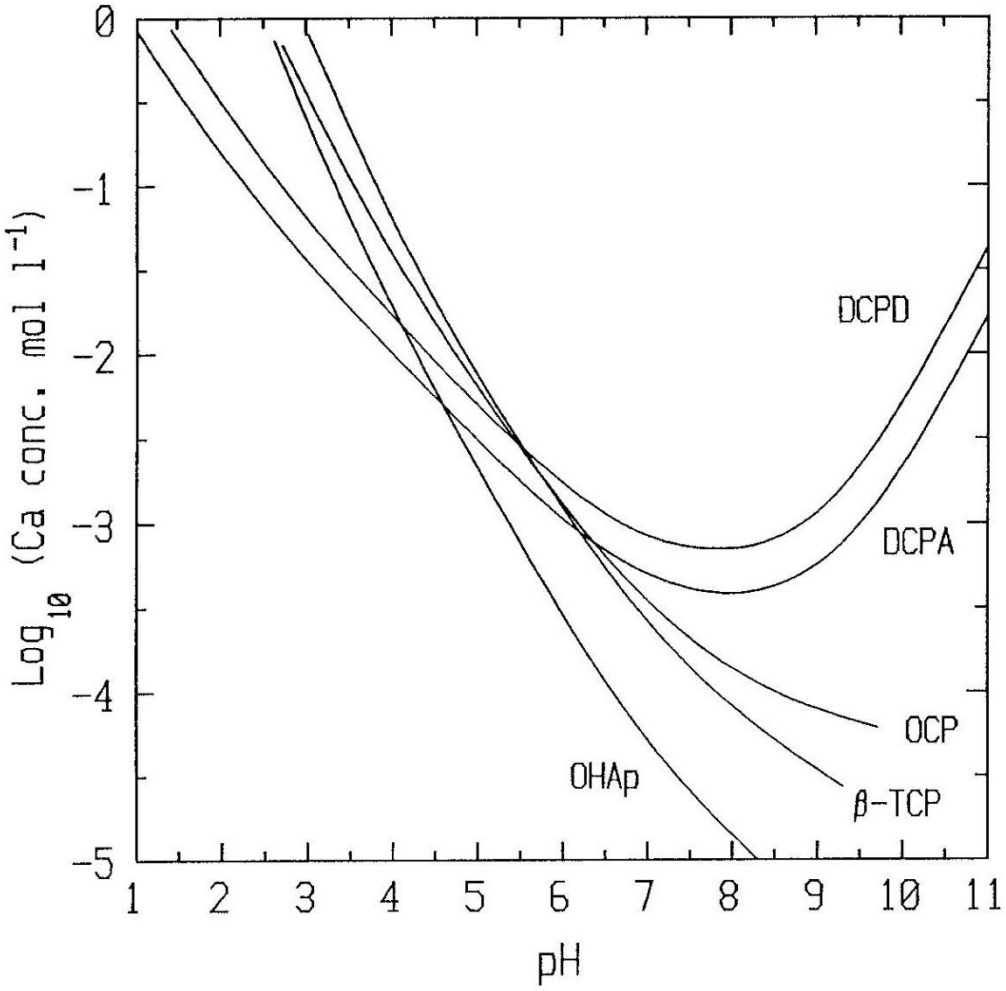

Figure 10: Solubility isotherms of calcium phosphates at 37°C calculated with the program RAMESES. Some of the abbreviations are given in Table 4, others signify: DCPA – dicalcium phosphate anhydrous (monetite), OHAp – hydroxyapatite. Note that normal body pH is just over 7. [17]

Stainless Steel [7]

The most common type of stainless steel used for implants is 316L (ASTM F138, F139) [18]. The inclusion of 2.25-3.00wt.% molybdenum improves salt water corrosion resistance, while the drop in carbon content from 0.08wt.% to 0.03wt.% maximum improves chloride solution corrosion resistance. Heat treatment and cold working can have a dramatic impact on the mechanical properties of stainless steel (see Table 5). The grain size of 316L should be 100 microns or less [18]. In humans, stainless steel is generally only used for temporary fixation, for example bone screws and nails, because it is still susceptible to corrosion in certain

situations, such as in highly stressed and oxygen depleted regions. Stainless steel is appealing for implant use in animals, however, due to their shorter lifetimes and the lower price compared to cobalt-chrome and titanium alloys.

Cobalt-Chromium Alloys [7]

The two cobalt-chromium alloys most often used to manufacture implants are CoCrMo (ASTM F75) and CoNiCrMo (ASTM F562). CoCrMo is castable and commonly used in dentistry and artificial joint applications, while CoNiCrMo is hot forged and usually used as the stem of joint replacements in legs. The properties of CoCrMo can be improved by hot isostatic pressing [18]. The addition of molybdenum gives the alloy better strength by hindering grain growth. Both alloys wear at similar rates, but CoNiCrMo alloy is not used as an articulating surface because it has inferior frictional properties. Cobalt-chromium alloys have the highest elastic moduli of common implant metals. The corrosion resistance of cobalt-chromium alloys is superior to stainless steel, but inferior to titanium alloy.

Titanium Alloys

Pure (98.9-99.6%) titanium (ASTM F67) has four different grades, correlating to a rise in impurity content [18]. These impurities, such as oxygen, carbon, and nitrogen, greatly affect the mechanical properties of titanium through interstitial solid solution strengthening (see Figure 11). Nitrogen gives about twice the strengthening effect per atom, but oxygen content varies the most between the grades, rising from 0.18% (grade 1) to 0.40% (grade 4). Hydrogen impurities can damage the ductility of titanium through the formation of hydrides [19]. Because of this the maximum amount of hydrogen allowed in titanium is 0.015wt%. Cold working has been shown to increase the fatigue strength of titanium [18]. The fatigue strength of pure titanium is far inferior to alloyed titanium, however (see Table 5).

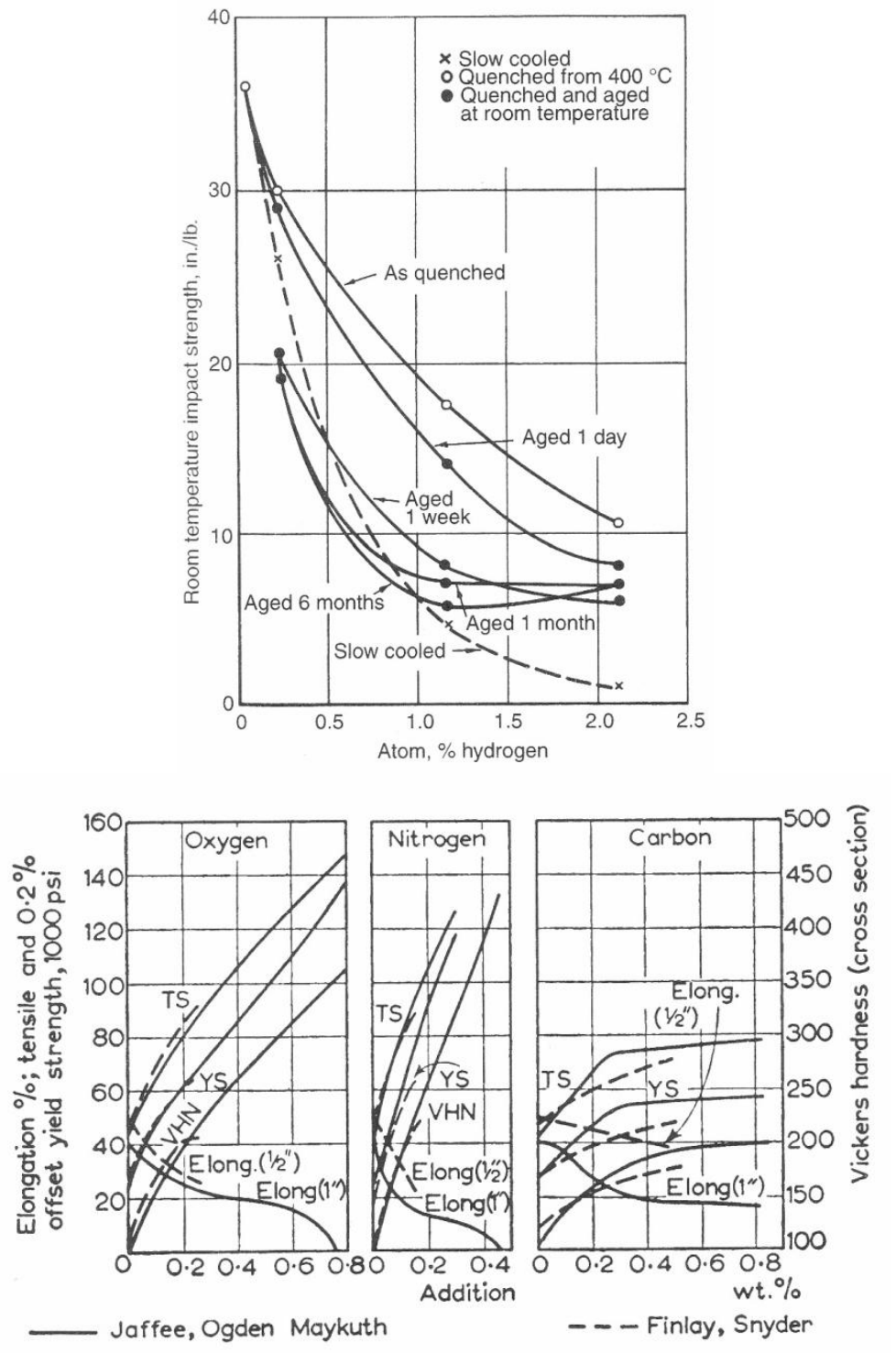

Figure 11: Effect of impurities on pure titanium. "Data of Jaffee are for samples annealed at 850°C; those of Finlay are for samples annealed at 700°C." TS and YS refer to tensile and yield strength respectively. [19]

Ti-6Al-4V (ASTM F136) is a very common titanium alloy used in implants [7]. Aluminum and vanadium are the largest alloying elements in Ti-6Al-4V at 5.5-6.5wt% and 3.5-4.5wt% respectively. The aluminum further stabilizes the stable, low temperature alpha phase (HCP) while vanadium stabilizes the metastable, high temperature beta phase (BCC) [19]. The alloy's properties can be better controlled by this two phase structure, with aluminum (alpha stabilizer) improving solid solution hardening and vanadium (beta stabilizer) lowering the temperature required for heat treatment.

Ti-6Al-4V has the largest specific strength, or strength per density, of any metallic implant material and also has the lowest elastic modulus [7]. Like pure titanium, Ti-6Al-4V is strongly affected by hydrogen, oxygen, carbon, and nitrogen impurities [18]. Ti-6Al-4V alloy is generally not used for temporary fixation because of its low shear strength, nor is it used as an articulating surface because it has a propensity to gall or seize [7]. Pure titanium and Ti-6Al-4V owe their exceptional corrosion resistance to the thin layer of TiO_2 on their surface.

Table 5: Typical mechanical properties of implant metals. [18]

Material	*ASTM designation*	*Condition*	*Young's modulus (GPa)*	*Yield strength (MPa)*	*Tensile strength (MPa)*	*Fatigue endurance limit (at 10^7 cycles, R = -1) (MPa)*
Stainless Steel	F745	Annealed	190	221	483	221-280
	F55, F56, F138, F139	Annealed	190	331	586	241-276
		30% Cold worked	190	792	930	310-448
		Cold forged	190	1213	1351	820
Co-Cr alloys	F75	As-cast/annealed	210	448-517	655-889	207-310
		Powder metallurgy product, hot isostatically pressed	253	841	1277	725-950
	F562	Hot forged	232	965-1000	1206	500
		Cold worked, aged	232	1500	1795	689-793
						(axial tension R= 0.05, 30Hz)
Ti alloys	F67	30% Cold-Worked Grade 4	110	485	760	300
	F136	Forged annealed	116	896	965	620
		Forged, heat treated	116	1034	1103	620-689

Note: $R = \frac{\sigma_{min}}{\sigma_{max}}$

ASTM F55 and F56 are withdrawn at this time.

Bone Cements

Bone cement is used during implantation to ensure the joint replacement is securely held in the bone cavity. Currently, the most commonly used bone cement is composed predominantly of poly(methylmethacrylate) (PMMA). Unfortunately, the failure rate of these bone cements is close to 10% within ten years post-operation [2]. After failure, a revision operation is necessary to re-secure or repair the implant, resulting in extra costs and pain to the patient. A significant improvement to, or a replacement of, PMMA bone cement would be a boon to joint replacement operations.

PMMA Cement

PMMA bone cement is mixed from a liquid component, containing methyl methacrylate monomer, and a solid powder, containing of poly(methylmethacrylate), each with several additives [7]. The liquid contains two additives to prevent early polymerization and improve curing of the cement at lower temperature and pressures than those used to produce dental implants. The solid component contains a radiopacifier and the free radical initiator. During mixing, the liquid wets the powder surface and polymerization occurs by a free radical process. The monomers grow into long chain polymers and polymerization continues until all of the initiator is consumed.

After mixing, PMMA bone cement must have a dough, or working, time of no more than 5 minutes, a setting time range of 5-15 minutes, and a final temperature less than 90°C [7]. Reported tensile and compressive strength values for different brands of PMMA bone cement vary from 13.2 to 48.2 MPa and 72.6 to 120 MPa [2]. Parks and Lakes [7] mention many intrinsic and extrinsic factors which may affect the final properties of PMMA bone cement, "composition of monomer and powder; powder particle size, shape, and distribution; liquid/powder ratio; mixing environment; mixing technique; and curing environment."

PMMA bone cement has several critical drawbacks [2]. Temperature rise during setting can cause necrosis of surrounding bone tissue if maximum temperature surpasses 56°C. Damage to cells can also begin at 48°C depending on exposure time. Reported max temperature values for the bone-bone cement interface vary substantially, but it is common for at least

one of the two given temperature criteria to be surpassed. Other concerns include monomer toxicity and negative foreign-body response to wear or fractured particles of the cement. This foreign-body response may cause aseptic loosening of the implant.

Ceramic Cement

Calcium Orthophosphate Cements [20]

These cements are created by mixing one or more calcium orthophosphate powder with an aqueous solution such as distilled water or phosphate-buffered saline. The mixed powders become a thick paste which can be molded into place and then set minutes later. The powder-to-liquid ratio of the cement controls the ease of injection and bioresorbability of the hardened cement. Dorozhkin points out the many advantages of calcium orthophosphate cements: fast setting time, excellent moldability, outstanding biocompatibility, easy manipulation, and perhaps most importantly, they are osteotransductive (i.e. the cement is slowly replaced by new bone tissue). Unfortunately, ceramic cements are brittle and as such are weak under tensile forces. This means that calcium orthophosphate cements must be used in conjunction with a metal implant or where load-bearing is not a criterion.

Calcium orthophosphate cements have been split into two major groups depending on the end product after setting. When the pH of the cement is greater than 4.2 either a poorly precipitated crystalline hydroxyapatite or calcium-deficient hydroxyapatite ($Ca_{10-x}(HPO_4)_x(PO_4)_{6-x}(OH)_{2-x}$ where $0<x<1$) forms, leading to this group's name of apatite cements. Brushite cements are formed at a pH below 4.2 and form dicalcium phosphate anhydrous (see Table 4 for formula). For both groups, the powders first dissolve into solution where the ions interact and then precipitate, resulting in the cement setting. According to Dorozhkin, "during precipitation the newly formed crystals grow and form a web of intermingling microneedles or microplatelets of the final products, thus provide a mechanical rigidity to the hardened cements." It should also be noted that calcium orthophosphate cements set primarily by two types of reactions: classical acid-base interaction and hydrolysis in an aqueous solution. The latter reaction uses a single metastable calcium orthophosphate powder, rather than a mixture.

Setting time is also an important characteristic that must be controlled. During surgery, the surgeon must have enough time to place the cement before it hardens, without having so much time that the operation is delayed. For calcium orthophosphate cements in orthopaedic applications, working time should be roughly 8 minutes and the cement should be set by 15 minutes.

Osteoceramic Cement

To improve the strength of calcium orthophosphate cements and make them a viable alternative to PMMA, composite cements have been developed. Calcium orthophosphate powders can be mixed with biocompatible calcium salts to create cements with various property changes [20]. Of note is a mixed calcium orthophosphate and calcium aluminate cement. A novel version of this cement, called osteoceramic cement (OC-cement), is composed of 33wt.% β-tricalcium phosphate and 66wt.% calcium aluminate, which is mixed with calcium chloride solution [21]. The components are mixed with vibration to improve mixing and expel trapped air. This cement has a working time of about 6 minutes and a setting time of 12-13.5 minutes at 37°C. Temperature increase during setting for OC-cement is much lower than for PMMA cement, with a maximum temperature increase of 15.5°C when tested at 22°C. The compressive strength of OC-cement over time can be seen below in Figure 12.

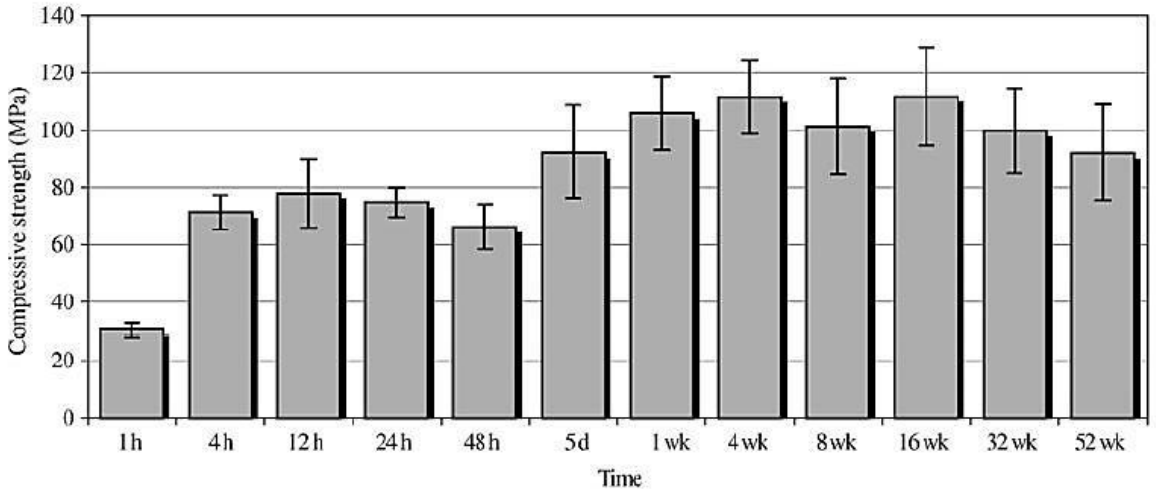

Figure 12: Compressive strength of OC-cement over time. [21]

Pull-out tests were performed to compare the interfacial shear strength of OC-cement to PMMA cement and it was determined that the differences between the mean strengths were not statistically significant; however the means for PMMA did slightly outperform the OC-cement at each time interval [21]. The tensile strength of OC-cement was found to be 7.02MPa and 11.34MPa at 24h and 1 week respectively, which is about 1/3-1/2 of common PMMA values.

During a 14 month test suspended in simulated physiological conditions, it was found that the mass of the OC-cement increased by 8.23% while its volume expanded 0.71% [22]. These changes are due to the hydration and conversion of the cement components. Roemhildt [22] suspects this slight increase in volume may enhance stability by preventing loosening, which is a problem in PMMA cements as they shrink after polymerization. OC-cement is dilatant and requires vibration during injection. This can be a benefit in certain circumstances, but does require a different procedure than standard PMMA cement protocols.

Design of Current Implants

The elbow implant discussed in this thesis was designed for use in canines; however, the ultimate goal is a design suitable for human use. Because of this, it is relevant to understand the functionality of currently used human and canine implants. The proposed ball centered elbow joint implant design will be modified for eventual human use after canine implementations have proven successful.

Canine Elbow Implant

As of 2009 the canine total elbow produced by BioMedtrix had been used for over 10 years, with approximately 750 implants shipped [23]. The implant utilizes an unconstrained design in two components: humeral and radioulnar (see Figure 13) [3]. The humeral component is made of 316L stainless steel, while the radioulnar component is formed from medical grade ultrahigh-molecular-weight polyethylene. On the humeral component, articulating surfaces were polished and other surfaces were bead blasted to give a rough finish. The radioulnar component has two stems to anchor it into the medullary cavities of both the radius and ulna.

The design allows for a theoretical range of 15° of flexion to 170° of extension; however it also calls for radioulnar synostosis, or bone fusion, which prevents useful rotation of the foot. The current success rate for this implant is 80% [23].

Figure 13: BioMedtrix total elbow implant showing cranial (left) and sagittal (right) views. [23]

A brief description of the surgical procedure described by Conzemius et al is as follows [3]. The elbow joint is approached caudolaterally and soft tissue is manipulated so that the radius and ulna can be moved to allow access to the humeral condyle. A hole is drilled through the trochlear notch into the medullary canal and the articulating surfaces of the humerus are removed. The excised bone is saved and used later to promote synostosis of the proximal radius and ulna. The articulating surfaces of the radius and ulna are then removed, followed by drilling holes into their medullary canals. PMMA cement is used to hold the implant stems in place in their respective medullary canals. Finally, the joint is put back together, the saved bone is placed between the radius and ulna, and the wound is closed.

Human Elbow Implant

The Coonrad-Morrey total elbow (see Figure 14) manufactured by Zimmer was used for 102 elbow arthroplasties in 86 patients over 13 years at a single institution [1]. According to a brochure available on the company website, the implant has an ulnar stem and a humeral stem each made of Tivanium® Ti-6Al-4V alloy, which are connected via a pin with an

ultrahigh-molecular-weight polyethylene bushing [24]. Portions of the stems are plasma spray coated to provide a rough surface to improve bone cement adherence. There is a flange on the proximal end of the humerus to hold a bone graft with the intention of improving the thickness of the bone locally. Shi et al found the five year success rate for this implant to be 72%, which is much lower than was found by the Mayo Clinic: 94.4% for rheumatoid arthritis and 80% for posttraumatic arthritis [1]. It is possible the broader definition of failure used by Shi et al may account for the difference. The most common source of failure in the study by Shi et al was implant loosening.

Figure 14: Zimmer Coonrad/Murrey total elbow. [24]

The surgical procedure for the human elbow implant is very similar to the canine procedure, but has several key differences. According to the surgical technique guide provided on Zimmer's website, the radius is mostly untouched during the procedure and a bone graft is wedged under the humeral flange; no bone graft is used to merge the proximal ends of the radius and ulna [24]. Because the implant is semiconstrained (i.e. humerus and ulna are connected by a pin), collateral ligaments do not need to be reattached.

MATERIALS AND METHODS

Zirconia-Toughened Alumina

The most important properties for the ball, radius base, and ulna base are fracture toughness and wear resistance. As mentioned previously, zirconia has better fracture toughness while alumina has the better ceramic-ceramic wear resistance. In order to avoid the drawbacks of zirconia, but gain its superior fracture strength, zirconia-toughened alumina (ZTA) was selected for the articulating surfaces. Low-temperature degradation (LTD) susceptibility is far less in ZTA because the zirconia phase is not interconnected throughout, so moisture diffusion is difficult, and the stiffer alumina matrix resists the transformation to the larger monoclinic phase [15].

It has been shown that alumina doped with 2.5wt.% zirconia has superior wear resistance to monolithic alumina at loads under 50N [25]. In fact, at a load of 20N ZTA wears an order of magnitude less than monolithic alumina. At loads higher than 50N, ZTA and monolithic alumina wear at similar rates. Not only does wear resistance increase, but also strength and toughness nearly doubled over the values for monolithic alumina.

Schehl, Díaz, and Torrecillas [26] investigated the mechanical properties of 5wt.% ZTA compared to high purity alumina. The results of this research can be seen in Table 6. It is easy to see that the fracture toughness of ZTA is far superior to alumina and approaches the fracture toughness values commonly seen for zirconia.

Table 6: Properties of high purity alumina and 5wt.% ZTA. Sintered at 1600°C for 2 hours. [26]

Material	***Young's Modulus (GPa)***	***Bending Strength (MPa)***	***Fracture Toughness K_{IC} ($MPa \cdot m^{1/2}$)***
High purity alumina	400	326	4.5
5wt.% ZTA	381	343	7.5

For this implant, alumina was doped with 5wt.% zirconia. The standard operating procedure for doping the alumina via a powder-alkoxide mixture (given in APPENDIX II) was developed using the specifications given by Schehl, Díaz, and Torrecillas [26]. Ceramic processing is described in a later section.

Osteoceramic

Osteoceramic is a ceramic-ceramic composite developed by Thomas McGee [27]. It is a 50-50 by volume mixture of calcium phosphate tribasic and $MgAl_2O_4$ spinel [28]. The calcium phosphate provides bioactivity while the spinel provides a strong backbone to maintain strength as the calcium phosphate phase interacts with living tissue. This two phase structure is critical for a successful ceramic implant because the flaw structure of a bioactive ceramic on its own cannot be controlled. In the case of osteoceramic, the spinel, a bioinert ceramic, maintains its original flaw structure as the calcium phosphate phase dissolves. Additionally, the constituent ions of spinel have significantly different atomic radii from calcium phosphate, which should limit solid solubility and allow an interconnected pore structure to form.

X-ray diffraction analysis and energy dispersive analysis on an SEM of osteoceramic sintered at 1500°C show two separate phases: α-tricalcium phosphate and $MgAl_2O_4$ spinel [28]. Electron micrographs of osteoceramic sintered at 1500°C are shown below in Figure 15 and Figure 16. The first image shows polished osteoceramic with the harder spinel phase at a higher elevation. The second image shows an osteoceramic surface treated with 8% ethylene diamine-tetraacetate (EDTA) for 20 minutes. This process etched away the calcium phosphate phase allowing the cubic spinel phase to be clearly seen.

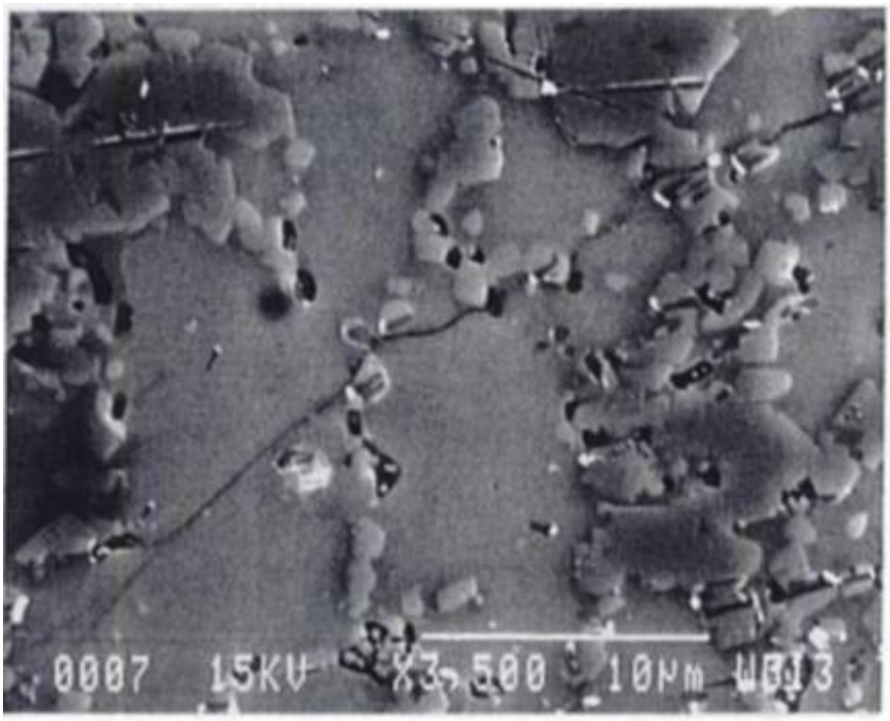

Figure 15: SEM micrograph of polished osteoceramic surface. (x3500) [28]

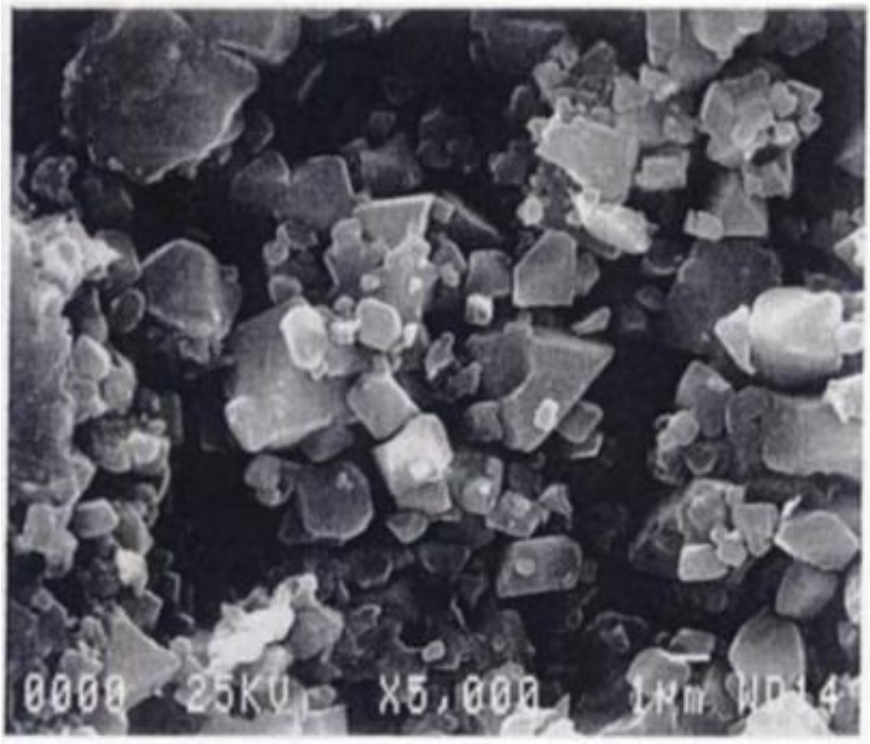

Figure 16: SEM micrograph of osteoceramic surface etched with EDTA. The calcium phosphate phase has been removed. (x5000) [28]

The compressive strength of 1450°C sintered osteoceramic is 199MPa [29]. It has a Young's Modulus of 114GPa which is very similar to that of titanium and its alloys. The porosity of osteoceramic is 8.32% and is well dispersed, with pore diameter ranging from 1.5-2.0 microns. Importantly, there is essentially no open porosity, which, when present, can wick or carry bodily fluids through the ceramic [28].

Keller [30] examined the in vitro biocompatibility of osteoceramic with osteoblast-like cells from rat pups. Three different surfaces of osteoceramic (polished, roughened by etching, and as-fired), along with a 24-well tissue culture plastic plate as a control, were exposed to these cells for 120 minutes. A micrograph of an osteoblast attached to the as-fired surface of osteoceramic can be seen in Figure 17. All surfaces had significant cell attachment, with the most on the rough surface and statistically equivalent attachment on the other three surfaces (see Figure 18). Keller notes that neither pure nor alloyed titanium have had osteoblast-like cell attachment greater than or equal to that of the tissue culture plastic plate.

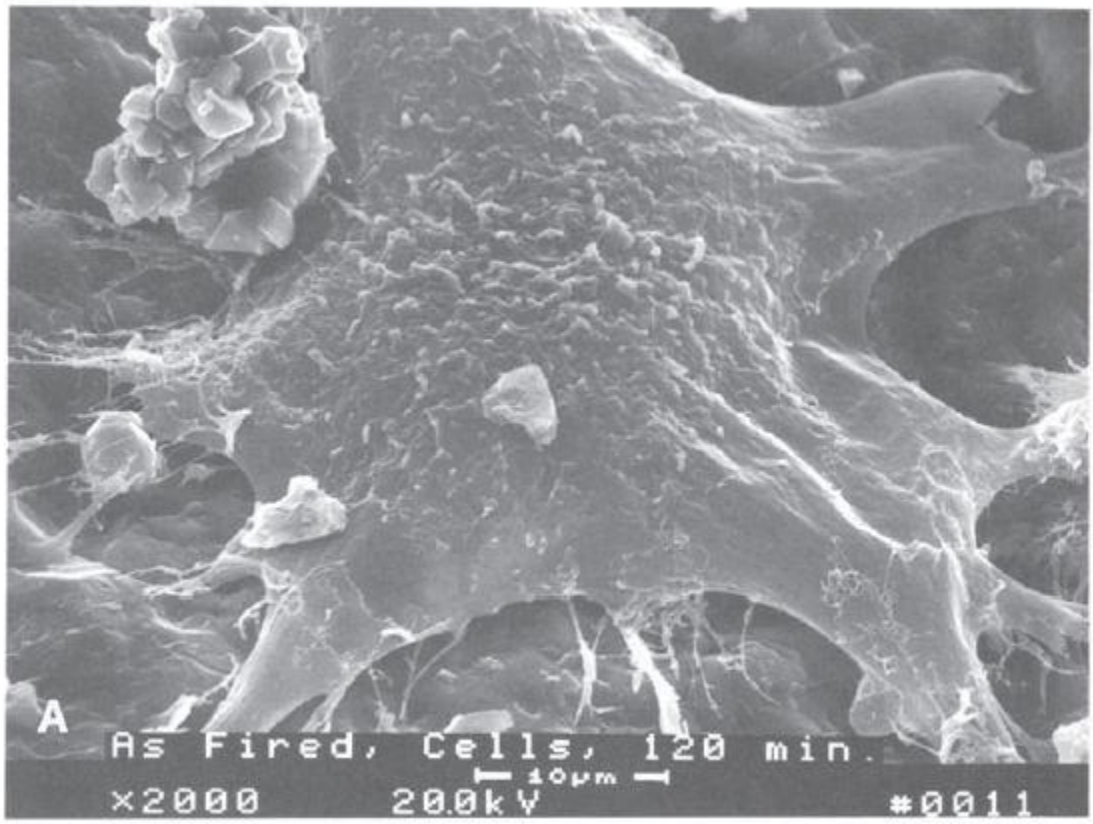

Figure 17: SEM micrograph of osteoblast-like cell on as-fired surface of osteoceramic. (x2000) [30]

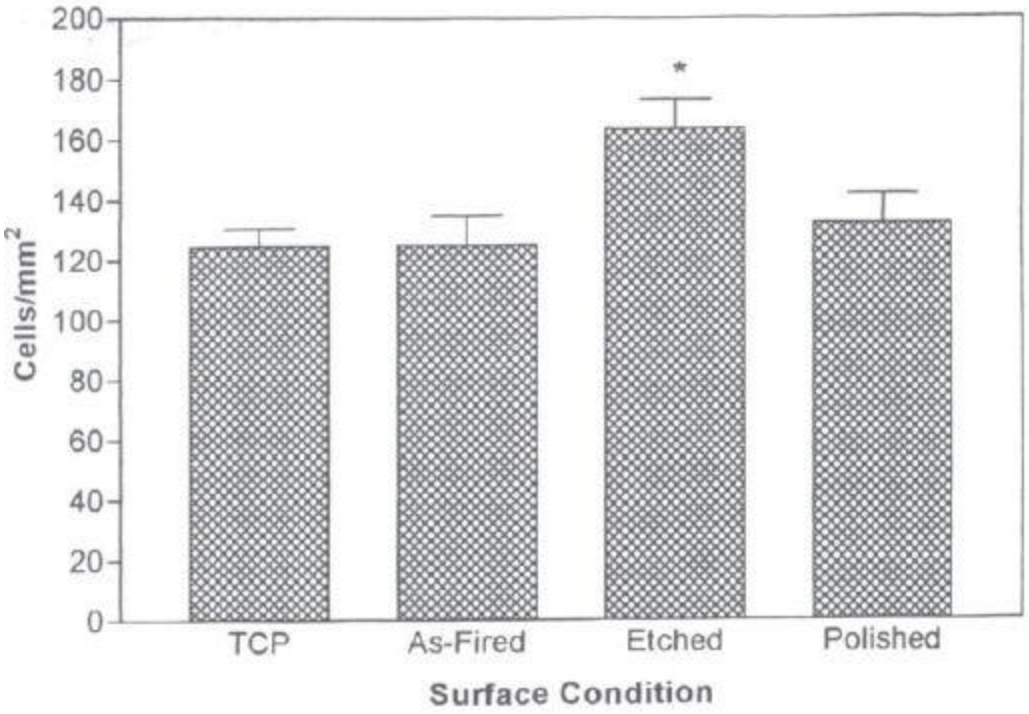

Figure 18: Osteoblast-like cell attachment to osteoceramic surfaces and control (TCP) after 120 minutes. Asterisk denotes statistically significant cell attachment. [30]

Two in vivo experiments in canines have proven that osteoceramic can induce bone growth and attachment [29]. The first was an osteoceramic bone graft with special geometry to guide bone regeneration and ensure bone attachment; new trabecular bone grew into its grooves and new compact bone grew around the implant. One dog had the implant for over eleven years and CAT scans showed that the compact bone of the operated limb was 50% of the unoperated limb, which lead to the conclusion that the implant and bone combined provide enough strength for a normal canine lifestyle.

The second experiment was induced diaphysis regeneration using osteoceramic tubes in the medullary canal to span a large gap in the diaphysis of nine canines [29]. The three control (no implant) dogs' femurs did not grow back together, but four other dogs had induced regeneration across the implant, with mineralized bone across the implant at the time of first radiograph (33-51 days depending on the dog). The two other dogs had bone bonding at the interface, although after removing half of the bone screws, induced bone regeneration across the implant took place in one of the dogs.

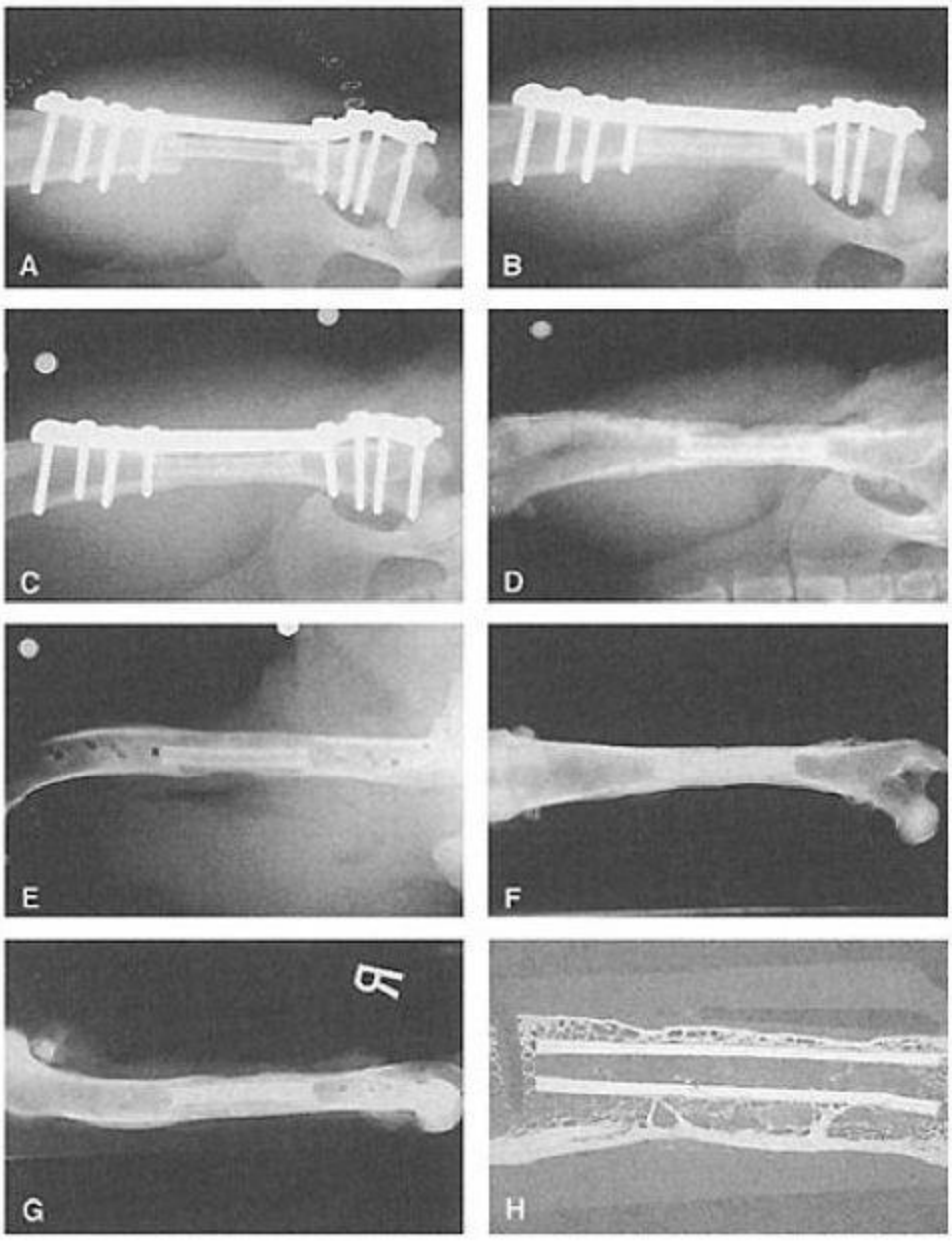

Figure 19: Microradiographs of a dog femur from the induced diaphysis regeneration experiment. [29]

(A) Postoperative

(B) 3 months

(C) 5 months

(D) and (E) 7 months immediately after removal of the plate and screws

(F) and (G) 11 months

(H) Medial-lateral section showing some transfer of load to the implant by trabecular bone.

Cold Isostatic Pressing

Both the osteoceramic and ZTA powders were formed into green bodies using cold isostatic pressing. Prepared tubes of powder (see APPENDIX IV) were isostatically pressed to 20000psi (137.9MPa). The formed rods measure approximately 100mm long by 20mm diameter.

Catheter Grade Osteoceramic Bone Cement

OC-cement has excellent properties; however, because it requires vibration to flow, its uses are diminished, especially because surgeons would prefer an injection method similar to the one used for PMMA cement. Catheter grade OC-cement (CGOC-cement) was developed to meet this need. CGOC-cement has properties very similar to those of OC-cement, but can be injected through a catheter tip syringe.

CGOC-cement is made by adding a small amount of flow-enhancing powders to the OC-cement formula. The powders are ground together in a mortar and pestle and then mixed with 2M $CaCl_2$ solution in a metal cup. The metal cup is vibrated during mixing to ensure thorough mixing. The cement is mixed for about two and a half minutes before it is scooped into a 60mL catheter tip syringe for injection (total time is about four minutes).

The strength of CGOC-cement has been tested in unpublished data. Cylinders of CGOC-cement with dimensions 18mm long by 12mm diameter were cast and set for 15 minutes. Then they were placed in a sealed bag with Ringer's solution and left in a hot water bath at 37°C until the designated testing time. After 45 minutes average compressive strength has surpassed 20MPa and after 24 hours strength has increased to close to 80MPa. Average compressive strength at 5 days is over 100MPa.

Materials Characterization

Linear Shrinkage, Density, and Porosity

Linear shrinkage and density were determined in tandem. Rods of Osteoceramic and ZTA were cold isostatic pressed and fired to machining temperature (1200°C for Osteoceramic and 1000°C for ZTA). The rods were machined into smooth cylinders and then cut into a handful of smaller cylinders with a Buehler Isomet low speed diamond saw. The heights, diameters, and masses of the cylinders were measured, allowing an approximate density to be calculated.

After firing the Osteoceramic and ZTA cylinders to 1450°C and 1650°C respectively, they were measured again and the results were compared to the previous measurements to calculate linear shrinkage. In the fully sintered state, the bulk density of the cylinders could be determined by use of an Archimedes' apparatus. The weight of each cylinder when all the pores are filled with water (saturated mass, m_s) and the weight when all the pores are filled with water and the cylinder is suspended in water (saturated suspended, m_{ss}) were determined in order to calculate multiple materials properties.

Tensile Strength

In order to determine the tensile strength of the ZTA ceramic, a diametral test was used. This test uses compression to create tensile forces that are at a maximum at the center of the disk, perpendicular to the compressive axis. Tensile strength was calculated from the max load by using the equation provided by Reed [31].

$$S_t = \frac{2P_f}{\pi dh}$$

Where S_t = engineering tensile strength (Pascals)

P_f = Max load (Newtons)

d = diameter (meters)

h = height (meters)

Disks of ZTA were made in the same manner as in the previous section: rods of ZTA were machined and then cut into disks with a slow speed diamond saw. Before firing to 1650°C

(fully sintered), the disks were polished to 600 grit. The fully fired disks were polished down to 6 micron with diamond paste. The height and diameter of each disk was then taken.

The disks were compressed with an Instron 4204 mechanical testing instrument. Clear tape was wrapped around each disk to hold the broken pieces together after failure. Each disk was set on its short edge and enclosed in a piece of cardboard to evenly distribute load over the contact surface. An aluminum block was used to ensure the disk was set vertically. The entire assembly (see Figure 20) was placed in a plastic bag to keep the broken pieces contained. The disk was kept vertical by applying hand pressure to the aluminum block while a small load (1-3kN) was placed on the disk to hold it in place. Then the aluminum block was removed and the test continued at a rate of 1mm/min until the disk broke.

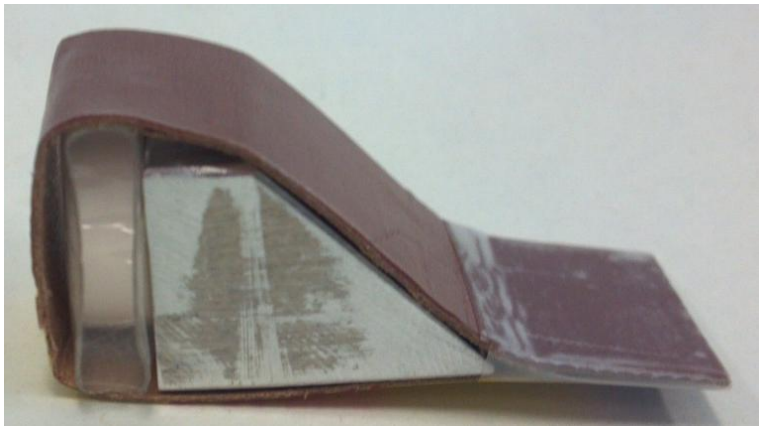

Figure 20: Diametral testing assembly

RESULTS AND DISCUSSION

Ceramic Processing

Originally the ZTA was mixed with water to create slip and cast on a plaster of Paris plate; however, the slip cast specimens did not have sufficient strength at 1000°C for machining. Isostatically pressed ZTA has sufficient strength for machining after firing to 1000°C. Higher sintering temperatures than 1000°C make machining very difficult. Osteoceramic rods were also formed via isostatic pressing. A description of the cold isostatic pressing procedure is given in a previous section (Page 35).

The osteoceramic and ZTA rods are then fired to 1200°C and 1000°C respectively (see APPENDIX V) to strengthen them for machining. After the specimens have been machined into appropriate oversized dimensions they are fired to their final temperature: 1450°C for osteoceramic and 1650°C for ZTA (see APPENDIX V). The dimensions of these fully fired specimens were used to machine the metal components to ensure proper fit.

Materials Characterization

Linear Shrinkage, Density and Porosity

Results and calculations used to determine a multitude of properties are shown in the table on the following page.

Table 7: Linear shrinkage and density of osteoceramic and ZTA.

Property	Equation	Osteoceramic	ZTA
Linear Shrinkage (machinable to fully sintered)	$\frac{L_m - L_{fs}}{L_{fs}} * 100$	17.8%	21.6%
Calculated Density (machinable)	$\frac{m_d}{\pi * r^2 * h}$	1.94 $\frac{g}{cm^3}$	2.27 $\frac{g}{cm^3}$
Calculated Density (fully sintered)	$\frac{m_d}{\pi * r^2 * h}$	3.13 $\frac{g}{cm^3}$	4.01 $\frac{g}{cm^3}$
True Density (ρ_t)	—	3.37[a] $\frac{g}{cm^3}$	4.05[b] $\frac{g}{cm^3}$
Bulk Density (ρ_b)	$\frac{m_d * \rho_L}{m_s - m_{ss}}$	3.12 $\frac{g}{cm^3}$	4.03 $\frac{g}{cm^3}$
Apparent Density (ρ_a)	$\frac{m_d * \rho_L}{m_d - m_{ss}}$	3.22 $\frac{g}{cm^3}$	4.04 $\frac{g}{cm^3}$
Open Pore Porosity ($\%OP$)	$\frac{m_s - m_d}{m_s - m_{ss}} * 100$	2.93%	0.24%
Closed Pore Porosity ($\%CP$)	$\left(1 - \frac{\rho_b}{\rho_t} - \frac{\%OP}{100}\right) * 100$	4.37%	0.25%
Percent Theoretical Density	$\frac{\rho_b}{\rho_t} * 100$	92.7%	99.5%
Number of Samples	—	9	11

Note: L_m is length after machining temperature firing.

L_{fs} is length after final firing (fully sintered).

m_d is the dry mass of a specimen.

ρ_L is the density of the submerging liquid.

[a]From [29]

[b]Calculated from relative specific volumes based on mass.

Tensile Strength

The diametral testing went smoothly; however, sample 6 broke while the small load (1-3kN) was applied. Average max load and tensile strength were found to be 23.05kN and 393MPa respectively. All of the samples broke catastrophically into many small pieces except for sample 4, which showed vertical lines of stress (see Figure 21). The shattering into tiny pieces was likely due to the fact that the sample held so much strain energy that an enormous number of surfaces had to be created to relieve the energy. The fracture pattern of sample 4 was expected and the initial fracture pattern of all the other samples would have started with a similar pattern before fracturing more to relieve excess energy. The results of the testing can be seen below in Table 8.

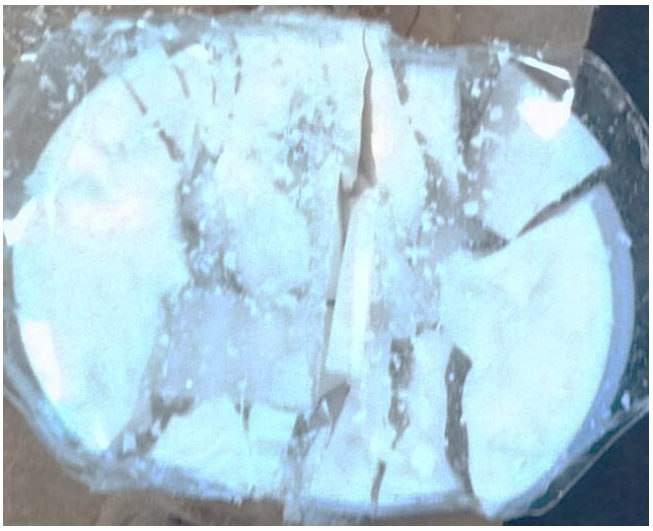

Figure 21: Diametral sample 4 after fracture.

Table 8: Diametral testing results.

Test No.	Diameter (mm)	Height (mm)	Max Load (kN)	Tensile Strength (MPa)
1	13.05	2.90	20.66	348
2	13.08	3.20	25.78	392
3	13.10	2.80	27.07	470
4	13.10	3.05	16.91	269
5	13.09	2.91	22.23	372
6	13.12	2.88	Broke during placement (<3kN)	
7	13.05	2.48	19.25	379
8	13.08	2.82	25.73	444
9	12.08	3.00	26.74	470

Scanning Electron Microscopy

One of the fractured pieces from the diametral testing was thermally etched at 1470°C for 15 minutes (recommended by [32]). The specimen was analyzed under an SEM to observe grain size and zirconia distribution, and to estimate experimental zirconia percentage using energy dispersive spectroscopy (EDS). The fracture surface of an unetched sample was also examined. In order to observe the samples at high magnification, a 5 micron layer of iridium was sputtered onto the surface of the samples to prevent charge build-up.

EDS estimated the weight percent of zirconia in alumina to be 4.98 to 6.38wt.% (average: 5.90wt.%). This is reasonably close to the target of 5wt.%, especially because the accuracy of EDS is lower at lower phase concentrations. Micrographs of the etched sample revealed that the zirconia phase is located within the grains as well as at grain boundaries (see Figure 22). The zirconia particles are roughly similar in size (~0.5 micron) and tend to be spherical when inside a grain and elongated when located on a grain boundary. By drawing lines on a micrograph and counting the grain boundaries, the alumina grain size was determined to be 1.5 microns. There is a wide variation in grain size, however, with a few grains larger than 10 microns and many less than 1 micron.

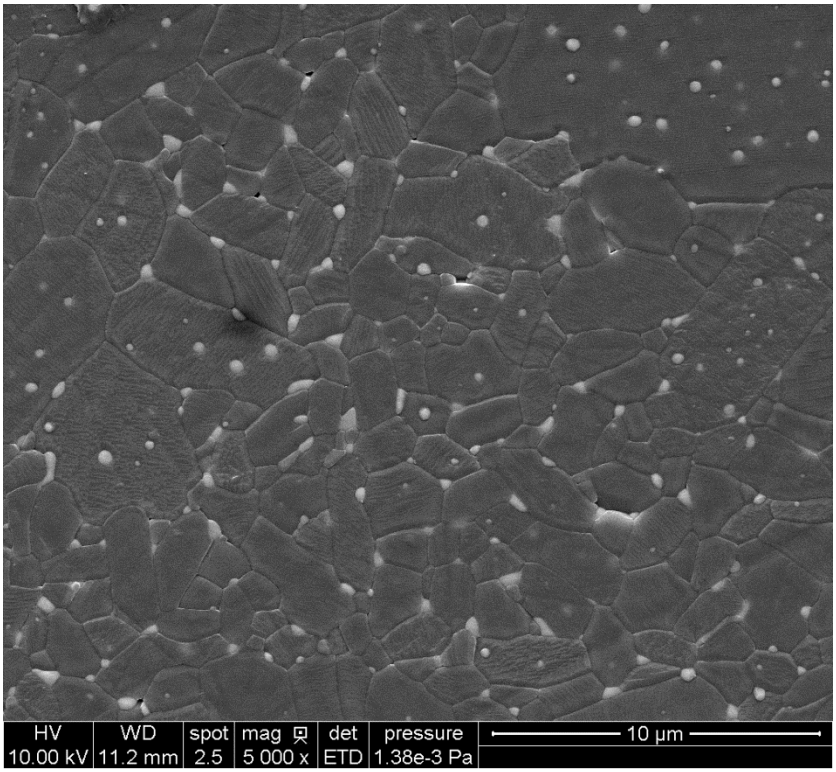

Figure 22: SEM micrograph of thermally etched ZTA. x5000

Analysis of the unetched fracture surface indicates predominantly intergranular fracture. It appears that a given crack has to change directions multiple times to propagate, which increases the energy of fracture. Figure 23, Figure 24, and Figure 25 each show the fracture surface at different magnifications.

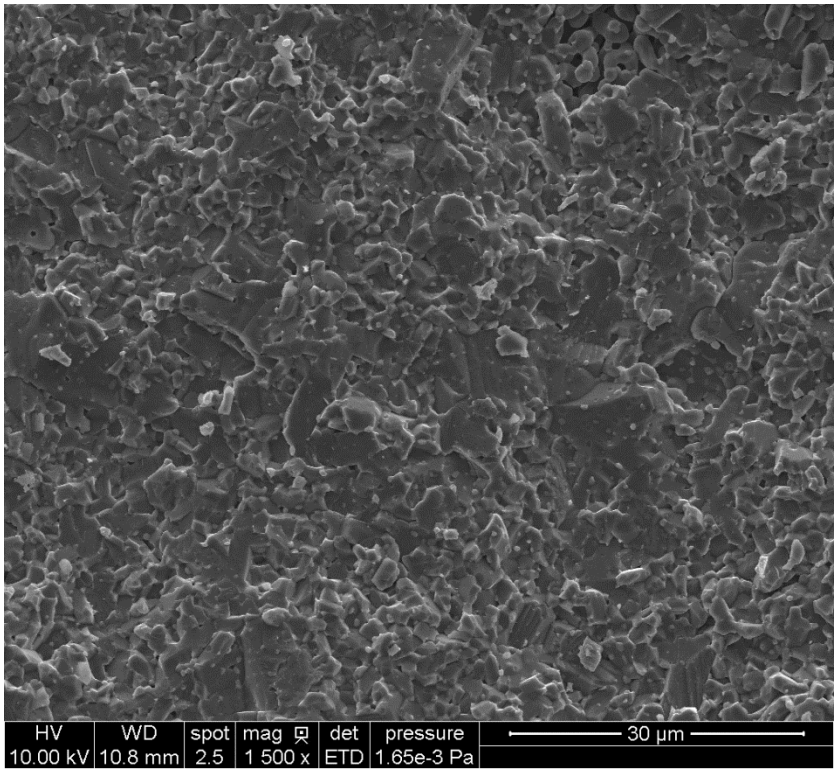

Figure 23: SEM micrograph of an unetched fracture surface. x1500

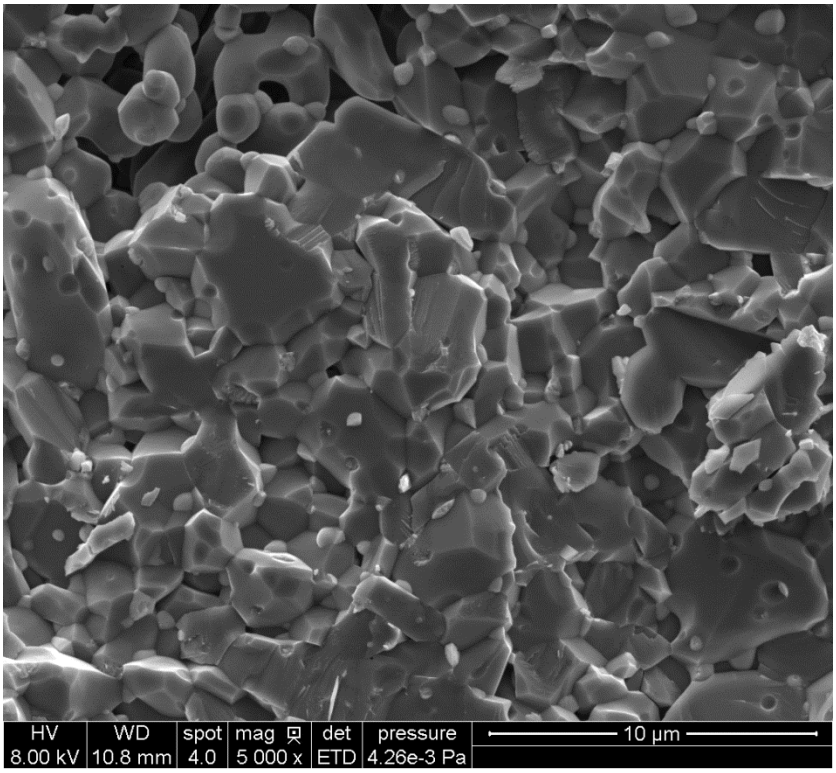

Figure 24: SEM micrograph of an unetched fracture surface. x5000

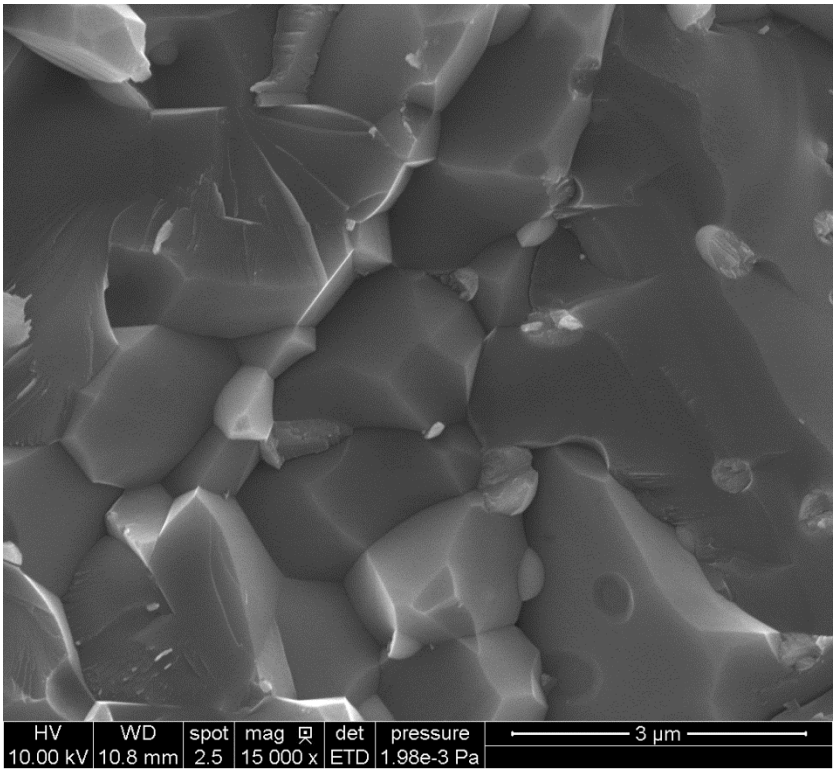

Figure 25: SEM micrograph of an unetched fracture surface. x15000

Design of the Implant Prototype

This new implant was designed to provide two primary improvements over current implants: reduce the amount of removed/damaged bone and return full/natural movement to the elbow joint while minimizing wear. In order to accomplish these goals, an unconstrained ceramic ball-centered design was adopted to provide proper arm rotation and bending while a revolutionary new surgical procedure, coupled with implant design, could significantly reduce the amount of excised bone. More discussion on the implant and surgical instrument design can be found in APPENDIX VI. The ball-centered elbow implant has three major subassemblies, one for each bone that makes up the elbow joint, and the schematics for each can be seen in APPENDIX VII.

Stainless steel (316L) was selected as the material for the metal components. The Ti-6Al-4V alloy would have been the superior metal due to its high fatigue and yield strength, along with its superior corrosion resistance; however, the cost of the material and its difficulty to machine made it nonviable for this canine prototype. Stainless steel has more than adequate

properties for a canine implant and is far less expensive and easier to machine than Ti-6Al-4V.

Zirconia-toughened alumina was selected for the articulating components of the implant. As discussed previously, ZTA provides improved fracture toughness over alumina and superb wear resistance. Zirconia doped with yttria was not selected because of low-temperature degradation (LTD) concerns. Bartolomé et al [25] noted that alumina-zirconia composites are "promising candidates for biomedical applications, for example, total joint replacement...".

The pre-final firing ceramic blanks were produced and prepared in the laboratory and then machined in the Black Engineering Machine Shop by the resident machinist. Metal parts were simply machined; however, features that held ceramic parts were not machined until final fired dimensions of the ceramic were measured. This was done to ensure that the ceramic component would fit into metal opening after shrinking to final dimensions.

Humeral Component

The humeral component can be more easily thought of as a ball and pin assembly. It has eight parts that work to hold a ZTA ball along the center of rotation of the humerus. The ball is designed to articulate with both the radius and ulna components and is held in place by two stainless steel nuts on a threaded stainless steel rod. Two sides of the ball are machined flat and parallel to ensure a tight fit by the nuts. One of the nuts has a thin tube extension out from its inner diameter to provide a smooth surface for the ball to rest on. The other nut screws onto the end of this thin tube to hold the ball in place. This ball and nut assembly can be rotated to easily move to a desired position on the threaded rod.

The threaded rod is secured to the humerus with two end caps. The end caps ride on the threaded shaft and have three small spikes to set it into the cancellous bone of the humerus. One of the end caps is threaded and is screwed into place against the humerus while the other is not threaded and is simply forced against the humerus. Each end cap also has an osteoceramic cylinder as in interface to improve fixation with bone bonding. The

osteoceramic has longitudinal grooves to prevent rotation and increase surface area for bone attachment. It is press-fitted inside the humerus when the end caps are set in place.

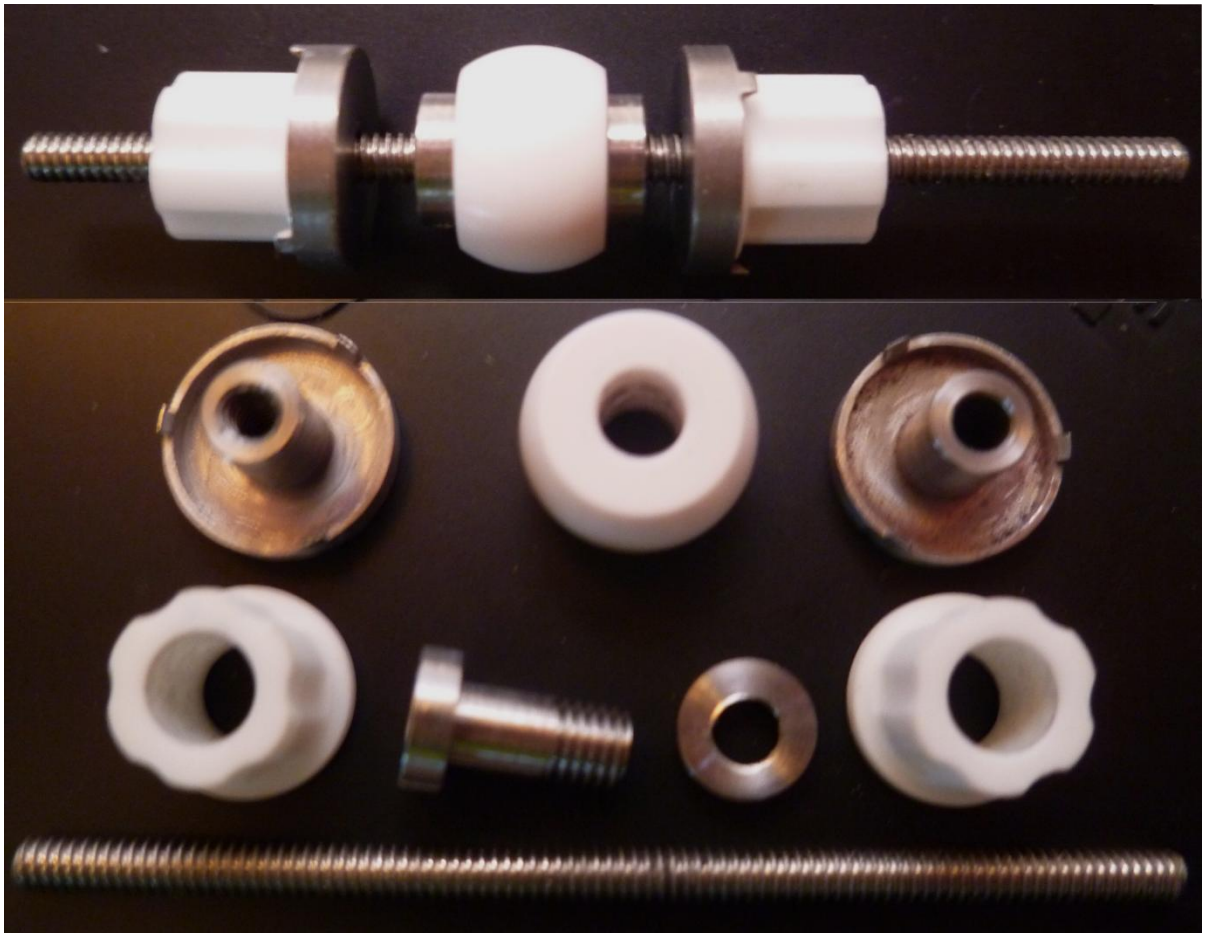

Figure 26: Humeral component assembled and disassembled into parts.

Radial Component

The radial component has five parts and transfers load from the ball of the humeral component to the radius. A cylinder of ZTA with a concave depression rests against the humeral ball and articulates smoothly against it. The cylinder is set into a stainless steel cup which has a cylindrical extension with internal threads. These threads allow the cup to be threaded onto a stainless steel base. A perfect fit against the humeral ball and ZTA cylinder is achieved by adjusting along this base. The base is secured against the radius with a bone screw and, like the humeral end caps, holds a cylinder of osteoceramic for bone attachment and long term stability.

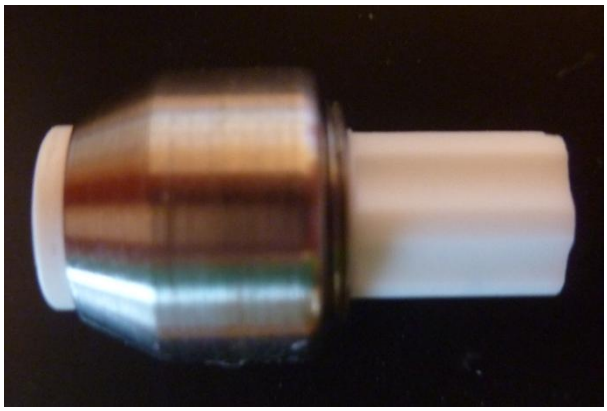

Figure 27: Radial component.

Ulnar Component

The ulnar component provides additional stability to the implant and supports some of the load from the humeral component. It has two parts, a ZTA surface to articulate with the humeral ball and a stainless steel "boat" that affixes it to the ulna. The "boat" has a long keel with two transverse holes drilled in it and a ridge to help it remain attached to the GCOC-cement that holds the component in place. The back of the keel is slightly tapered so it is more difficult to remove once it is set in place. The sides of the "boat" have curved flanges to follow the curvature of the cut in the ulna and to hold cement. There is a hole in the front of the "boat" which is designed to hold a standard bone screw. This bone screw will be angled toward the olecranon and will provide additional stabilization, especially until the cement has fully set.

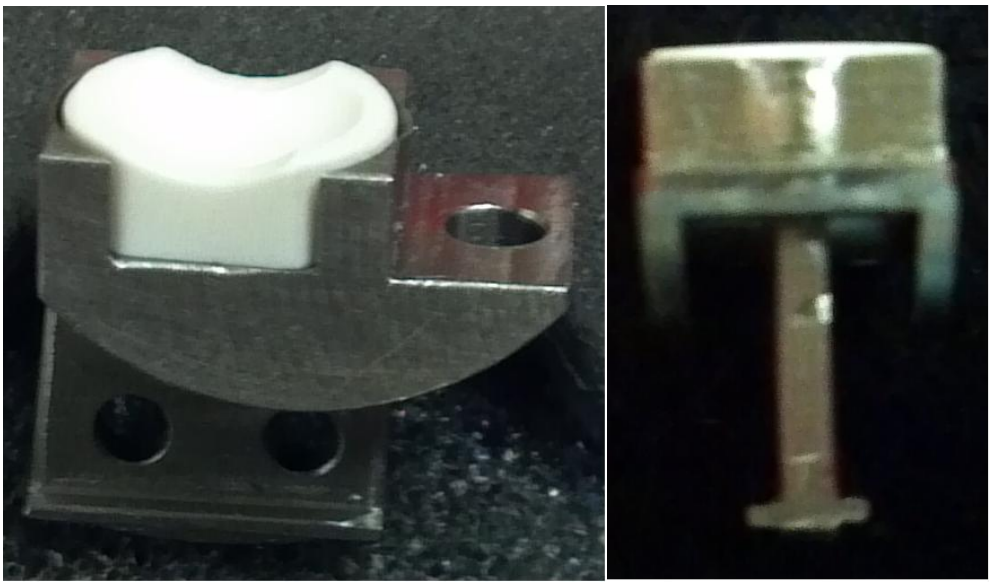

Figure 28: Ulnar component side and front views.

Cadaver Canine Joint Examination

Dr. William Hoefle, DVM, MS; an orthopaedic surgeon at the Iowa State University College of Veterinary Medicine and the Lloyd Veterinary Medical Center was consulted to determine the viability of the constructed elbow implant. He was initially optimistic, but was concerned that after removal of the trochlea, the lateral condyle may not have sufficient support from ball and pin assembly to prevent fracture. The proposed surgical procedure, which would approach the elbow joint cranially instead of caudally, was also discussed. He felt that the presence of nerves, veins/arteries, and muscle tissue on the cranial side would make such a procedure difficult, but he was willing to investigate the possibility on a cadaver canine elbow.

The cranial approach on the cadaver was successful; however a significant amount of muscle tissue was separated and the exposure provided was not large enough for the designed cutting apparatus. Widening the exposure would increase the possibility of damage to the radial nerve. Dr. Hoefle suggested an alternative approach, similar to one used commonly in surgical practice, where the joint is approached caudally and an osteotomy is done in the proximal ulna just below the elbow joint. This allows easy access to all of the elbow joint and afterwards the proximal ulna is reattached with a pin and a figure-eight of tension band wire.

While examining the articulation of the humerus and radius (with the proximal ulna displaced), Dr. Hoefle expressed concern that the radius would articulate too far laterally on the humerus. This might require that more of the lateral condyle be removed, further weakening boney support. He did not say it was impossible, but did suggest that some alterations of the implant might alleviate this potential problem.

SUMMARY AND CONCLUSIONS

The ball-centered elbow joint replacement prototype design called for a strong metal backbone with wear resistant articulating surfaces. Bone bonding at the implant-tissue interface was also desired. Stainless steel, ZTA, and osteoceramic were selected to meet these criteria. The designed parts were manufactured and assembled into a working prototype.

ZTA can be relatively easily produced and sintered into a dense ceramic with high fracture toughness, good tensile strength, excellent wear resistance, and almost no negative impact to other material properties. When alumina is prepared by CeramTec for their Biolox® products (most prevalent total hip replacement ceramic), a hot isostatic pressing operation is required [33,34]. It appears that the powder-alkoxide mixing and open air sintering method used in this research to create a nanocomposite ZTA is a viable alternative to the costly hot isostatic pressing process currently implemented by CeramTec.

Many compromises had to be made to create the ball-centered elbow joint replacement prototype detailed in this research. The original design was envisioned for humans and many changes had to be made to adapt the (now current) design to a canine elbow. After reviewing a cadaver canine elbow joint, another change may be required. The location of the ZTA ball needs to move laterally, which may require envisioning a new humeral component instead of the ball and pin assembly. This may be advantageous, because there is some concern that the 3/32” pin would not be strong enough to for long term use.

The ultimate goal is to create an elbow replacement for use in humans. The current ball and pin design for the humerus may still be viable for this application; however, it is likely that two balls would be necessary because humans have more forearm rotation than canines. A human elbow is significantly larger than a canine’s so it is possible that some of the current concerns could be resolved simply because there is more space and bone stock. The entire implant could easily be upscaled which would should alleviate concerns about the size of the pin.

It is strongly believed that the use of osteoceramic and CGOC-cement will significantly decrease the likelihood of aseptic loosening. Bone will bond to the osteoceramic to create a stronger bone-implant interface than is currently seen in implants that use PMMA bone cement. CGOC-cement can provide similar strength to PMMA bone cement and, like its precursor OC-cement, does not increase in temperature enough to cause tissue necrosis. Neither osteoceramic nor CGOC-cement will cause a negative foreign body response if wear or fracture particles are released, a huge advantage over PMMA bone cement.

It is recommended that the implant be tested in a cadaver canine as soon as a humeral component alternative is designed. The short- and long-term strength of the bone-osteoceramic interface needs to be investigated to determine if more or less osteoceramic is required to achieve adequate strength. After a successful cadaver experiment, an in vivo study should be performed. Before implantation in vivo, ZTA components will need to be polished against each other to ensure a matched, smooth surface to provide maximum wear resistance.

APPENDIX I: ALUMINA

Table 9: Properties of single-crystal α-Al_2O_3. [32]

Melting point (°C)	-	2051 ± 9.7	
Density (g/cm^3)	-	3.98	
Refractive index	ordinary ray (c-axis)	1.768	
	extraordinary ray	1.760	
Hardness (GPa) HV500g	parallel to c	19.03	
	perpendicular to c	21.56	
Young's modulus (GPa) parallel to c	at RT	435	
	1000C	386	
RT compressive strength (GPa)	-	2	
Bend Strength (MPa)	along c-axis at RT	1035	
	perpendicular to c-axis at RT	760	
	at 45d to c at 600°C	325	
	at 45d to c at 1000°C	587	
Thermal expansion coefficient (10^{-6}/K)	0-127°C	6.26 (*ll* c)	5.51 (perp. c)
	0-527°C	7.96	7.15
	0-1127°C	8.84	7.96
	0-1727°C	9.18	8.30
Thermal conductivity (W/m*K)	RT	36	
	100°C	28.9	
	500°C	10.5	
	1100°C	5.9	
	1900°C	6.3	

Table 10: Properties of Ceralox APA-0.5 alumina. [35]

Product	Al_2O_3 Purity	D-90 µm	D-50 µm	D-10 µm	Surface Area, m^2/g
APA-0.5	99.96%	0.5	0.3	0.2	8.0

APPENDIX II: ZIRCONIA-TOUGHENED ALUMINA SYNTHESIS

Note: The following was developed following the procedure given by Schehl et al [26].

1. Pour ~400mL of 200 proof ethanol into a 1000mL beaker. Insert a 3 inch magnetic stirring rod and place the beaker on a hot/stirring plate set to stirring level 8 or 9 (heat off for now).
2. Carefully add 190.00g of Ceralox APA-0.5 alumina (no MgO) (see APPENDIX I) into the beaker and disperse the powder in the ethanol. Add more ethanol and/or adjust stirring speed as necessary to keep the powder dispersed.
3. Pour ~40mL of Sigma-Aldrich zirconium(IV) propoxide solution (70wt.% in 1-propanol) into a 50mL beaker. Use a 10mL graduated cylinder to transfer 36.2mL into a 100mL mix beaker.
4. Measure out ~18mL of 200 proof ethanol in the same 10mL graduated cylinder. Pour into the 100mL mix beaker with zirconium solution. Gently swirl beaker.
5. Pour or use a disposable pipette to transfer the zirconium/ethanol solution from the mix beaker to the 1000mL beaker containing ethanol/alumina slurry. Add the solution slowly—do not spill or splash solution out of the beaker. Pour any remaining solution into the 1000mL beaker if it cannot be reached with the pipette.
6. Turn on the hot plate to level 5 and check that the stirring speed is sufficient.
7. As the ethanol evaporates residue will be left on the wall of the beaker. Use a rubber spatula to scrape this residue back into the slurry or rinse the walls of the beaker with ethanol. If a rubber spatula is used, rinse it with ethanol to make sure any residue on the spatula goes back into the beaker. Once all of the ethanol has evaporated or the magnetic stirring rod no longer spins (this should take 4-6 hours), remove the magnetic stirring rod and scrape any powder/slurry back into the beaker. It is OK if the slurry is not completely dry.
8. Cover the beaker with a watchglass and set it in the large oven at ~120°C overnight to remove any traces of ethanol.
9. Break up the white chunks in the bottom of the beaker and transfer the powder/chunks into a 500mL wide mouth plastic jar. Add ¼” cylindrical alumina

grinding media until the jar is about 2/3 full and then run it in the vibration mill for 4 hours. Sift the powder through a 40 mesh sieve.

10. Place the milled powder in an alumina crucible and cover it with a platinum foil square. Set the crucible in a furnace and calcine at 850°C. Store.

Thermal Treatment of Powder at 850°C

1. Ramp to 500°C at 100°C/hour
2. Dwell 2 hours
3. Ramp to 850°C at 200°C/hour
4. Dwell 2 hours
5. Ramp to 20°C at 100°C/hour
6. End

APPENDIX III: OSTEOCERAMIC SYNTHESIS

Material	***Description/Manufacturer***	***Amount***
Spinel	S30CR Spinel, Baikowski	313.03 g
$Ca_3(PO_4)_2$	Mallinckrodt, Rhodia- TCP	277.19 g
PEG 600	Carbowax Sentry	17.90 g
Darvan	Na Darvan #7, Vanderbilt	26.60 g
DI H_2O	De-Ionized Water	520 mL

Place the above materials into a one gallon ball mill jar, adding DI H_2O first, then Darvan and PEG 600, followed by the dry materials. Use ¾" cylindrical alumina grinding media and mill for 12-18 hours. Remove slurry from the mill and dry on a plaster slab, making sure you place cheesecloth on the plaster slab before placing the OC on it.

After 2-3 days, remove the OC from the plaster slab and dry it in a drying oven overnight. Grind the dry OC to -80 mesh with a mortar and pestle.

APPENDIX IV: COLD ISOSTATIC PRESSING SPECIMEN PREPARATION

Remember: It is best to have the powders as tightly packed as possible before isostatic pressing. This will help you get a sample closer to the size of the mold, and increase the chances of a successful (high green density) press.

1. Cap one end of an oil-resistant rubber tube (approximately 6 in. long) of desired diameter with a rubber stopper. Be sure that there are no holes in the stopper or rubber tube. Clamp the tube onto the stopper with a hose clamp.
2. Place the rubber tube into a plastic sleeve of appropriate size. The sleeve will help keep the sample a consistent shape and diameter.
3. To pack the sample, place some powder into the tube and use a steel rod to tamp the powders until densely packed. Repeat until the tube is filled. Be sure to leave room for a stopper at the end of the tube.
4. Remove the plastic sleeve from the sample and cap the end of the tube with a second rubber stopper and clamp. Take care to prevent trapping air inside the tube.
5. Make sure that your sample is air tight so that no oil contaminates the sample and no powder gets into the oil. The specimen is now ready for cold isostatic pressing.

APPENDIX V: FIRING PROGRAMS

1200°C Osteoceramic Firing Program:

1. Ramp up to 1200°C at 100°C/hr
2. Dwell at 1200°C for 2 hours
3. Ramp down to 20°C at 100°C/hr
4. End

1000°C ZTA Firing Program:

1. Ramp up to 1000°C at 100°C/hr
2. Dwell at 1000°C for 30 minutes
3. Ramp down to 20°C at 100°C/hr
4. End

1450°C Osteoceramic Firing Program:

1. Ramp up to 1450°C at 100°C/hr
2. Dwell at 1450°C for 2 hours
3. Ramp down to 20°C at 100°C/hr
4. End

1650°C ZTA Firing program:

1. Ramp up to 1600°C at 100°C/hr
2. Ramp up to 1650°C at 60°C/hr
3. Dwell at 1650°C for 15 minutes
4. Ramp down to 20°C at 100°C/hr
5. End

APPENDIX VI: IMPLANT AND SURGICAL INSTRUMENTS DESIGN

The following section was written by Dr. Thomas McGee:

Recent improvements in laparoscopic repair of synovial joints, minimized access incisions, and robotic surgical tools have improved surgical performance, reduced pain, and improved recovery. However, joint replacements have not change much since Charley first used PMMA cement and polyethylene in 1948. Many attempts to replace the articulating components have failed because bone does not bond to the metals, plastics, and ceramics that are still in use.

The osteoceramic elbow joint design is revolutionary in nature because it does not remove the function nature of the lower (distal) end of the humerus. That bone is one of the densest in the skeleton. By preserving it, much less trauma occurs. The anterior approach to the articulating components makes it possible to replace just the articulating components. It is revolutionary also because bone will bond to the osteoceramic component and cause the implant to be anchored firmly in the bone.

Replacing conventional polyethylene (PE) wear components prevents failure due to PE particles in the synovial cavity that cause inflammatory response, pain, and loosening.

The new design is controversial because of the difficulty in surgical performance without damage to muscles, tendons, and nerves. The surgical procedure requires removal of a section of the trochlea (humerus bearing surface) and replacing it with a ZTA ball at the center of rotation for the joint, and also at, or near, the center of rotation of the radius. This may not be possible but must be evaluated experimentally.

If this approach is practical, special surgical instruments are needed to maintain the stability of the centers of rotation during the procedure. These have been designed and manufactured. They will be used in a simulated surgery using a cadaver foreleg in the near future. An alternative approach suggested by Dr. Hoefle will also be evaluated.

APPENDIX VII: ELBOW IMPLANT SCHEMATICS

The following pages show the specific dimensions of each part of the elbow joint replacement prototype. Gray parts are stainless steel, teal parts are ZTA, and gold parts are osteoceramic. NF threads refers to the standard national fine thread size and all dimensions are in inches. Fully sintered dimensions are given for the ceramic components. The dimensions given to the machinist can be determined by increasing the listed dimensions by 17.8% for osteoceramic and 21.6% for ZTA.

Figures 29-34: Humeral component parts

Figures 35-38: Radial component parts

Figures 39-40: Ulnar component parts

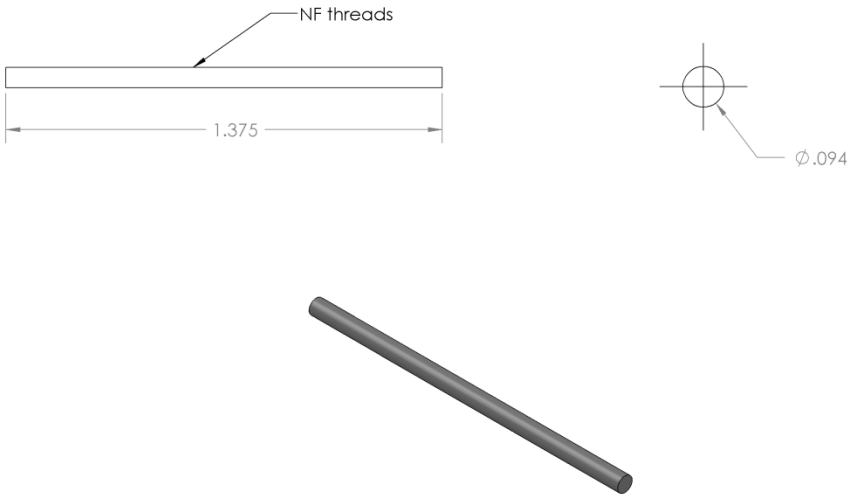

Figure 29: Threaded rod for humeral component.

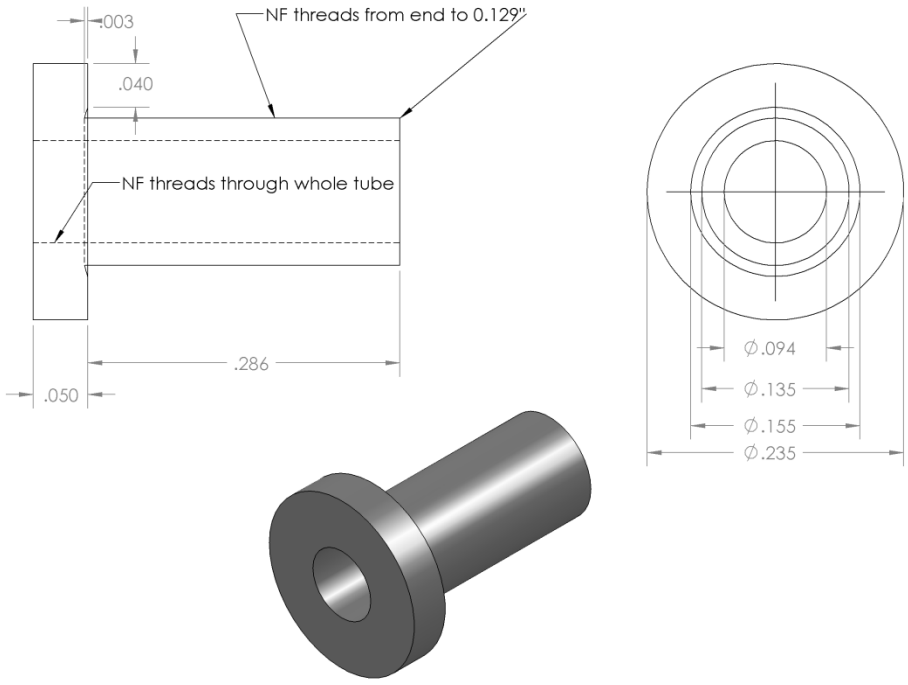

Figure 30: Ball core tube for humeral component.

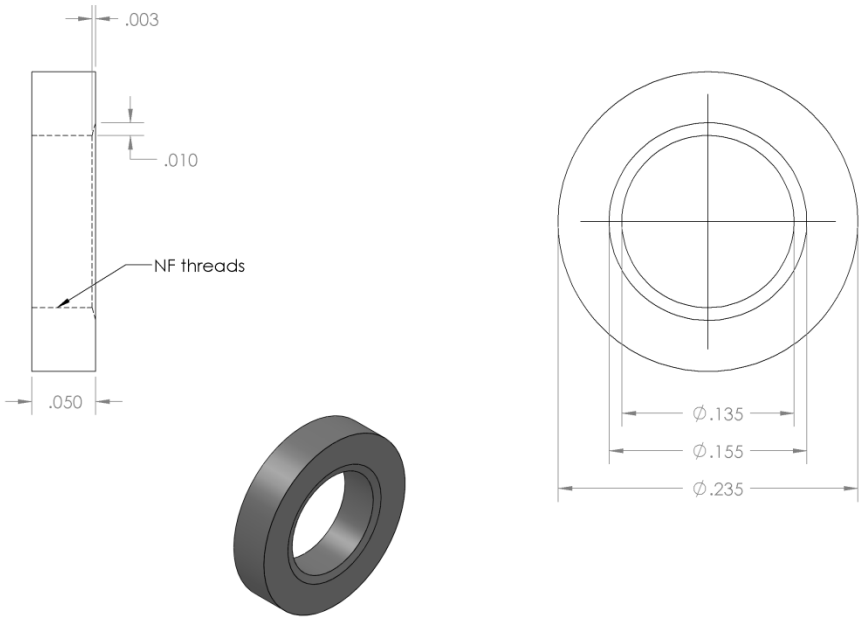

Nut for Humeral Component

Figure 31: Nut for humeral component.

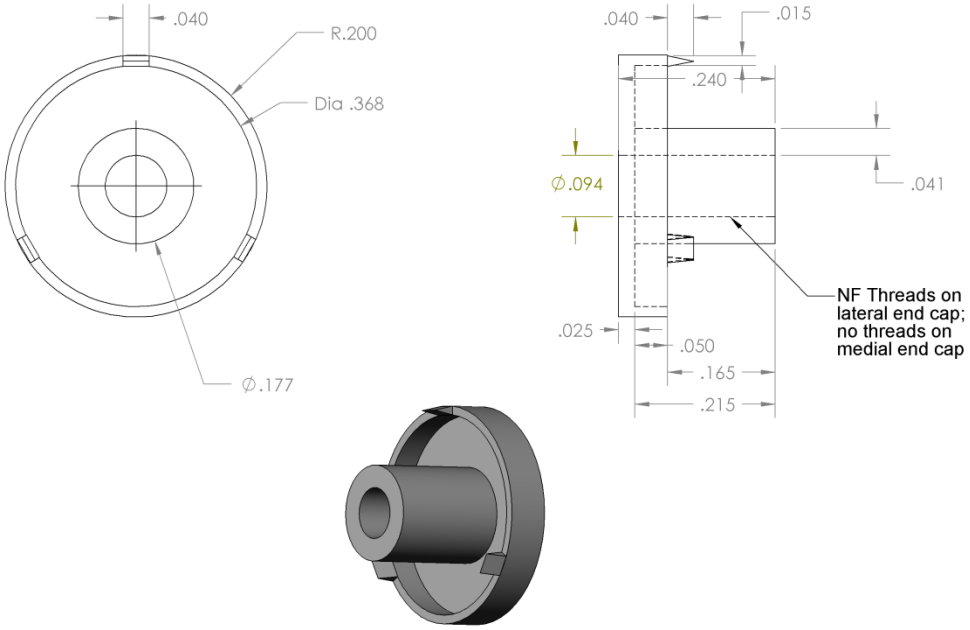

End Cap for Humeral Component

Figure 32: End cap for humeral component.

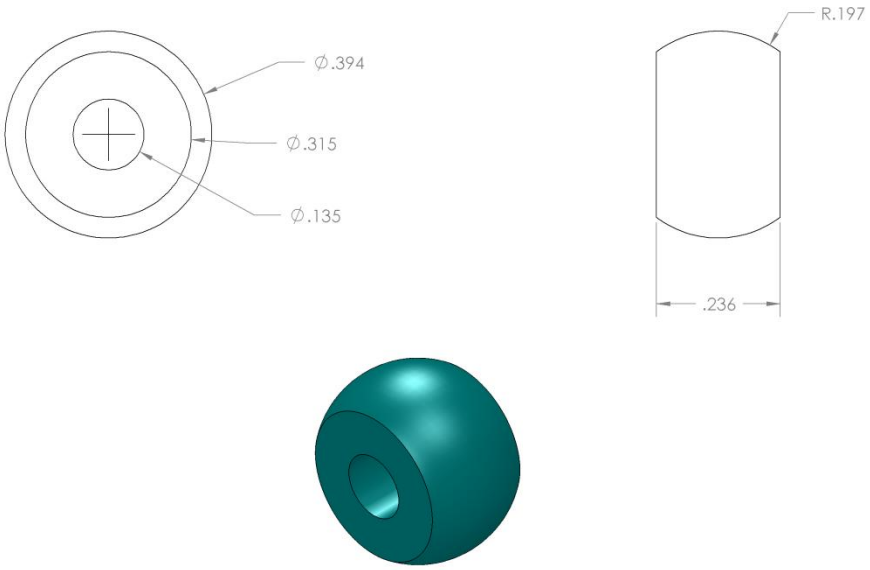

ZTA Ball for Humeral Component

Figure 33: ZTA ball for humeral component.

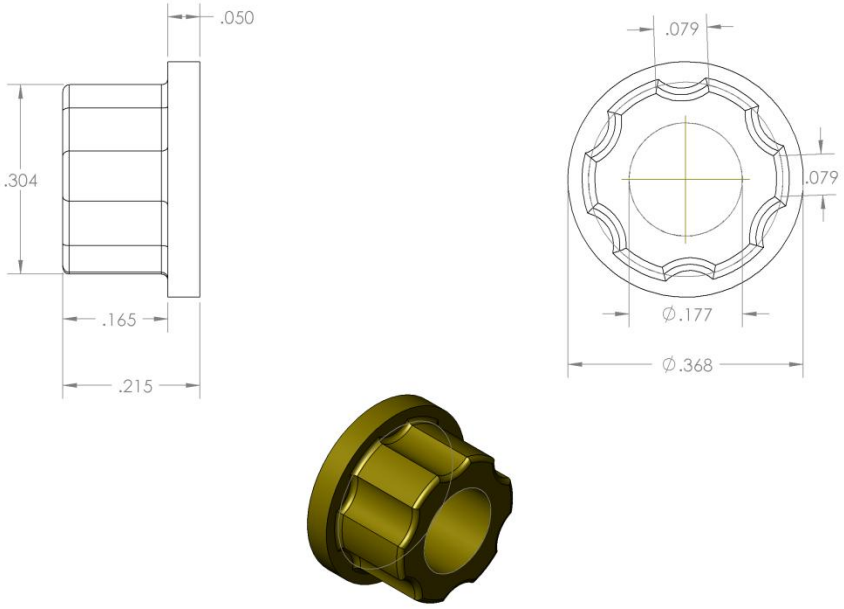

Osteoceramic Sleeve for Humeral End Caps

Figure 34: Osteoceramic sleeve for humeral end caps.

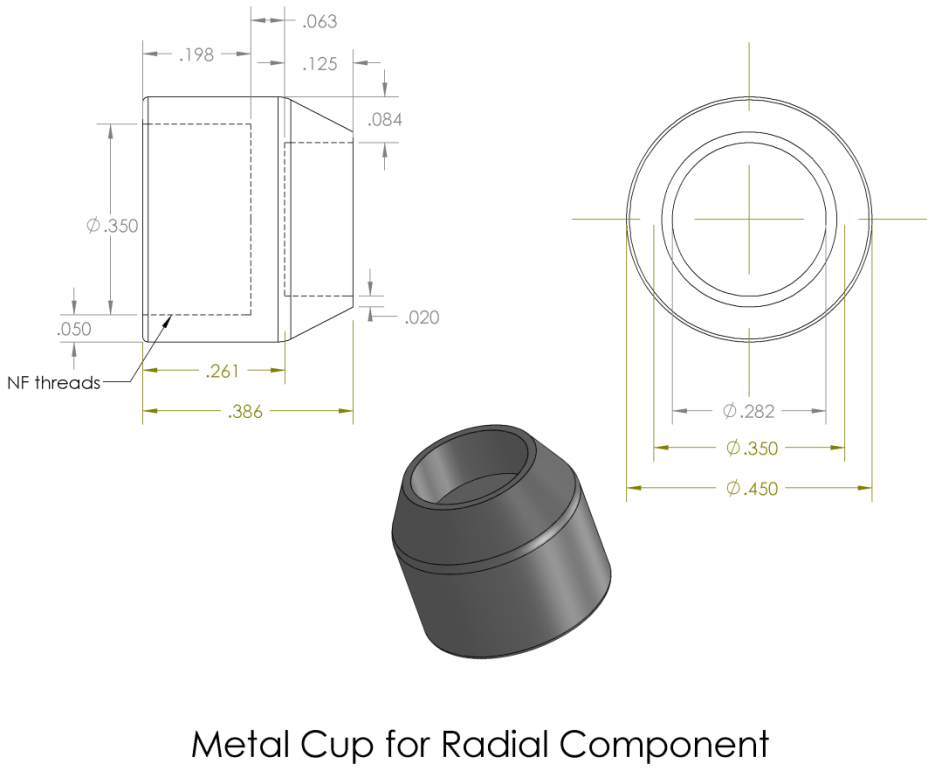

Figure 35: Metal cup for radial component.

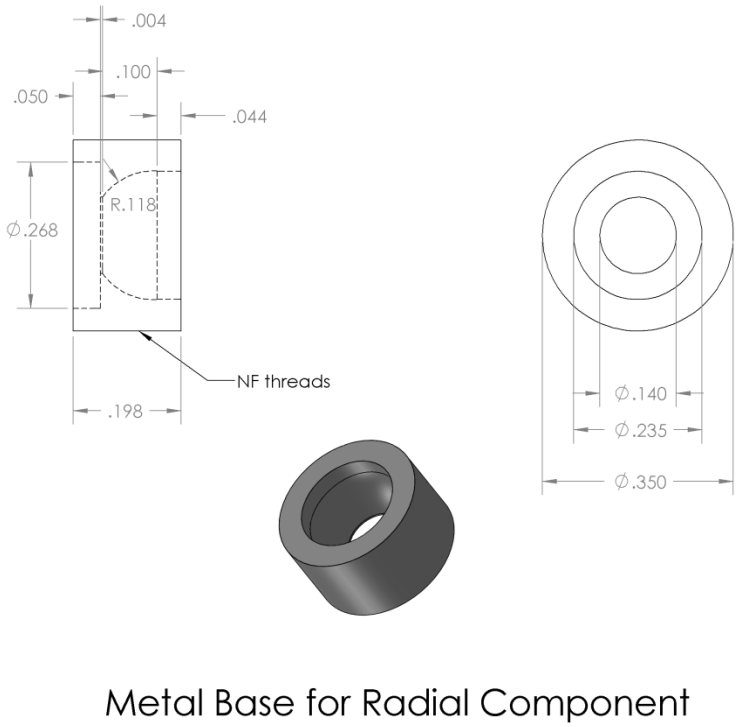

Figure 36: Metal base for radial component.

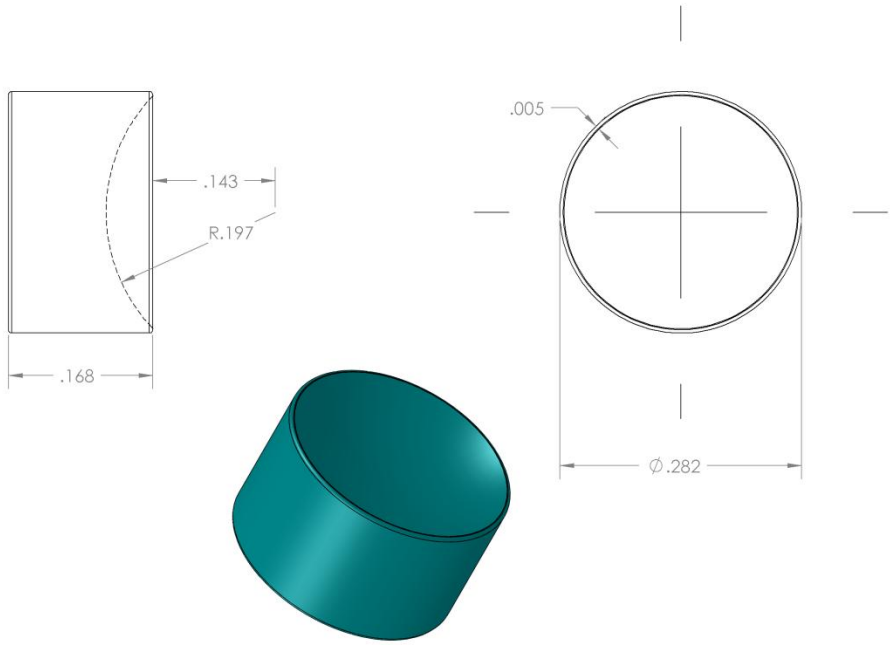

Figure 37: ZTA articulating surface for radial component.

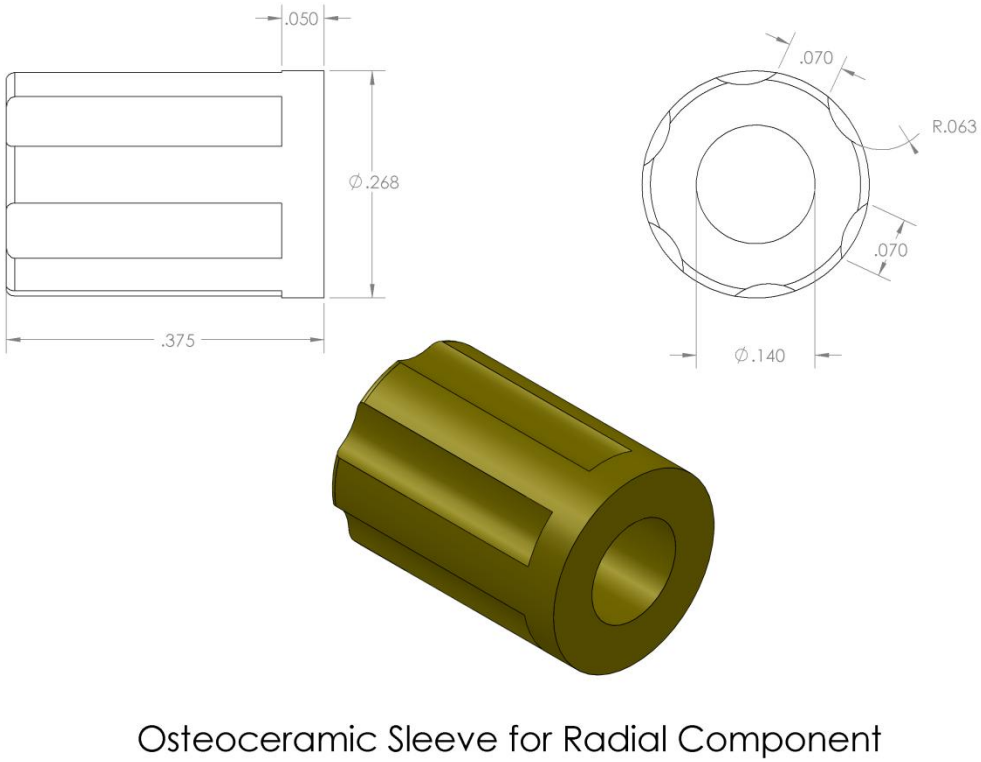

Figure 38: Osteoceramic sleeve for radial component

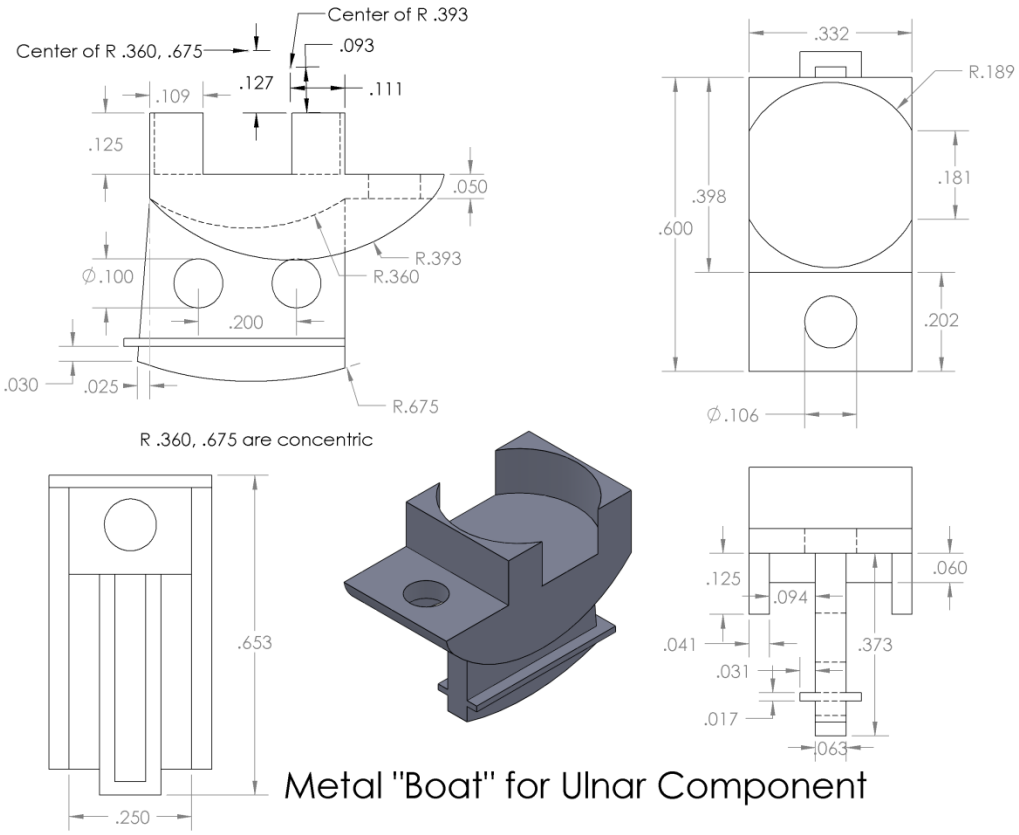

Figure 39: Metal "boat" for ulnar component.

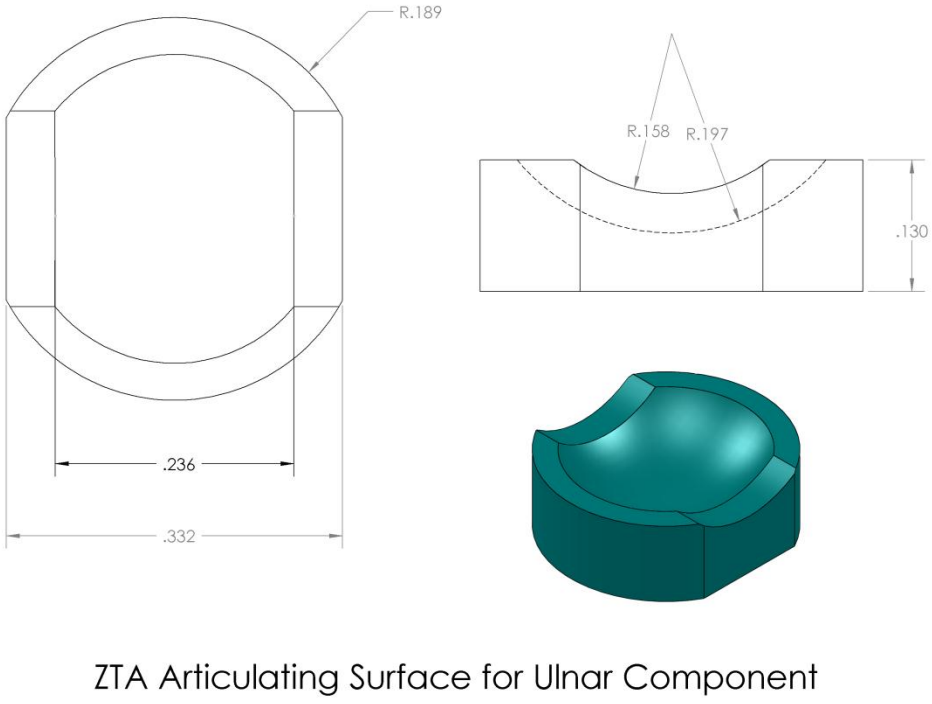

Figure 40: ZTA articulating surface for ulnar component.

BIBLIOGRAPHY

[1] Lewis L. Shi, David Zurakowski, Deryk G. Jones, Mark J. Koris, and Thomas S. Thornhill, "Semiconstrained Primary and Revision Total Elbow Arthroplasty with Use of the Coonrad-Morrey Prosthesis," *The Journal of Bone and Joint Surgery*, vol. 89, no. 7, pp. 1467-1475, July 2007.

[2] J. A. Planell, M. M. Vila, F. J. Gil, and F. C. M. Driessens, "Acrylic Bone Cements," in *Encyclopedic Handbook of Biomaterials and Bioengineering, Part B: Applications*, Donald L. Wise et al., Eds. New York, NY, USA: Marcel Dekker Inc., 1995, vol. 2, ch. 32, pp. 879-921.

[3] Michael G. Conzemius, Rhonda L. Aper, and Christopher M. Hill, "Evalution of a Canine Toal-Elbow Arthroplasty System: A Preliminary Study in Normal Dogs," *Veterinary Surgery*, vol. 30, no. 1, pp. 11-20, January 2001.

[4] H. R. Denny, "The Canine Elbow," *British Veterinary Journal*, vol. 143, no. 1, pp. 1-20, January-February 1987.

[5] Elain Nicpon Marieb, *Human Anatomy & Physiology*, 4th ed. Redwood City, CA, USA: Benjamin/Cummings Pub., 1998.

[6] Yuehuei H. An and Richard J. Friedman, "Animal Selections in Orthopaedic Research," in *Animal Models in Orthopaedic Research*, Yuehuei H. An and Richard J. Friedman, Eds. Boca Raton, FL, USA: CRC Press LLC, 1999, ch. 3, pp. 39-57.

[7] Joon Park and R. S. Lakes, *Biomaterials: An Introduction*, 3rd ed. New York, NY, USA: Springer Science+Business Media, 2007.

[8] J. T. Tiffit, "The Organic Matrix of Bone Tissue," in *Fundamental and Clinical Bone Physiology*, M. R. Urist, Ed. Philadelphia, PA, USA: J.B. Lippincott, 1980, ch. 3.

[9] Bonnie J. Smith, *Canine Anatomy*. Philadelphia, PA, USA: Lippincott Williams & Wilkins, 1999.

[10] Julian Seifter, David Sloane, and Austin Ratner, *Concepts in Medical Physiology*. Philadelphia, PA, USA: Lippincott Williams & Wilkins, 2005.

[11] Yuehuei H. An and Robert A. Draughn, "Mechanical Properties and Testing Methods of Bone," in *Animal Models in Orthopaedic Research*, Yuehuei H. An and Richard J. Friedman, Eds. Boca Raton, FL, USA: CRC Press, 1999, ch. 8, pp. 139-164.

[12] Hiroshi Yamada, *Strength of Biological Materials*, F. Gaynor Evans, Ed. Baltimore,

MD, USA: Williams & Wilkins, 1970.

[13] Stavros C. Manolagas and Robert L. Jilka, "Bone Marrow, Cytokines, and Bone Remodeling: Emerging Insights into the Pathophysiology of Osteoporosis," *The New England Journal of Medicine*, vol. 332, no. 5, pp. 305-311, 1995.

[14] Larry L. Hench and Serena Best, "Ceramics, Glasses, and Glass-Ceramics," in *Biomaterials Science: An Introduction to Materials in Medicine*, 2nd ed., Buddy D. Ratner et al., Eds. San Diego, CA, USA: Elsevier Academic Press, 2004, ch. 2.10, pp. 153-170.

[15] Jérôme Chevalier, Laurent Gremillard, Anil V. Virkar, and David R. Clarke, "The Tetragonal-Monoclinic Transformation in Zirconia: Lessons Learned and Future Trends," *Journal of the American Ceramic Society*, vol. 92, no. 9, pp. 1901-1920, September 2009.

[16] G. Willmann, "Zirconia: a medical-grade material?," in *Bioceramics*, P. Ducheyne and D. Christiansen, Eds. Oxford, UK: Pergamon, 1993, vol. 6, pp. 271-276.

[17] J. C. Elliott, *Structure and Chemistry of the Apatites and Other Calcium Orthophosphates*. Amsterdam, The Netherlands: Elsevier Science B.V., 1994.

[18] John B. Brunski, "Metals," in *Biomaterials Science: An Introduction to Materials in Medicine*, 2nd ed., Buddy D. Ratner et al., Eds. San Diego, CA, USA: Elsevier Academic Press, 2004, ch. 2.9, pp. 137-153.

[19] Matthew J. Donachie Jr., *Titanium: a technical guide*, 2nd ed. Materials Park, OH, USA: ASM International, 2000.

[20] Sergey V. Dorozhkin, "Calcium orthophosphate cements for biomedical application," *J Mater Sci*, vol. 43, no. 9, pp. 3028-3057, March 2008.

[21] M. L. Roemhildt, T. D. McGee, and S. D. Wagner, "Novel calcium phosphate composite bone cement: strength and bonding properties," *Journal of Materials Science: Materials in Medicine*, vol. 14, no. 2, pp. 137-141, 2003.

[22] M. L. Roemhildt, S. D. Wagner, and T. D. McGee, "Characterization of a novel calcium phosphate composite bone cement: Flow, setting, and aging properties," *Journal of Materials Science: Materials in Medicine*, vol. 17, no. 11, pp. 1127-1132, September 2005.

[23] Mike Conzemius, "Nonconstrained Elbow Replacement in Dogs," *Veterinary Surgery*, vol. 38, no. 2, pp. 279-284, February 2009.

[24] Zimmer. Zimmer. [Online]. http://www.zimmer.com/en-US/hcp/elbow/product/coonrad-morrey-elbow-system.jspx

[25] José F. Bartolomé et al., "Alumina/Zirconia Micro/Nanocomposites: A New Material for Biomedical Applications With Superior Sliding Wear Resistance," *Journal of the American Ceramic Society*, vol. 90, no. 10, pp. 3177-3184, October 2007.

[26] M. Schehl, L.A. Díaz, and R. Torrecillas, "Alumina nanocomposites from powder-alkoxide mixtures," *Acta Materialia*, vol. 50, no. 5, pp. 1125-1139, March 2002.

[27] Thomas D. McGee, "Artificial Bone or Tooth Prosthesis Material," 3787900, January 29, 1974.

[28] Thomas D. McGee, Ann M. Graves, Katherine S. Tweden, and Gabriele G. Niederauer, "A Biologically Active Ceramic Material with Enduring Strength," in *Encyclopedic Handbook of Biomaterials and Bioengineering, Part A: Materials*, Donald L. Wise et al., Eds. New York, NY, USA: Marcel Dekker Inc., 1995, vol. 2, ch. 42, pp. 1413-1427.

[29] C. E. Olson, S. D. Wagner, and T. D. McGee, "Guided Diaphysis Regeneration," in *Biomaterials in Orthopedics*, Michael J. Yaszemski et al., Eds. New York, NY, USA: Marcel Dekker, Inc., 2004, ch. 9, pp. 195-212.

[30] John C. Keller, Jeannie G. Collins, Gabrielle G. Niederauer, and Thomas D. McGee, "In vitro attachment of osteoblast-like cells to osteoceramic materials," *Dental Materials*, vol. 13, no. 1, pp. 62-68, January 1997.

[31] James S. Reed, *Principles of Ceramics Processing*, 2nd ed. New York, NY, USA: John Wiley & Sons, Inc., 1995.

[32] William E. Lee and W. Mark Rainforth, *Ceramic Microstructures Property Control by Processing*, 1st ed. London, UK: Chapman & Hall, 1994.

[33] S. Affatato, F. Traina, M. De Fine, S. Carmignato, and A. Toni, "Alumina-on-alumina hip implants a wear study of retrieved components," *The Journal of Bone and Joint Surgery*, vol. 94-B, no. 1, pp. 37-42, August 2011.

[34] CeramTec. (2012, March) CeramicTec the Ceramic Experts. [Online]. http://www.ceramtec.com/

[35] Sasol North America, Inc. - Ceralox Division. (2005, January) Sasol: reaching new frontiers. [Online]. http://www.ceralox.com/hpa.asp

ACKNOWLEDGEMENTS

I would like to thank Dr. Richard LeSar and Dr. William Hoefle for their support and willingness to be part of this research. I also want to thank Dr. William Hoefle for providing invaluable insight into surgical practice. My sincerest gratitude goes to Kevin Brownfield, the machinist who not only managed to create the small and complex implant components, but also provided useful feedback and recommendations. I must also thank Warren Straszheim from the Materials Analysis Research Laboratory for his skill at scanning electron microscopy. Special thanks go to Ryan Franck and John Solomon for their previous work and expertise in osteoceramic and ceramic cements respectively.

Finally, I especially want to thank Dr. Thomas McGee for his time, patience, and enthusiasm for this research. His desire to expand my knowledge as much as possible will always be appreciated.